

Thesis for the degree of Doctor of Philosophy

**SPECTROSCOPIC STUDIES OF BIOMOLECULES  
CONFINED IN SELF-ASSEMBLED  
NANOSTRUCTURES**

**NILS CARLSSON**

Department of Chemical and Biological Engineering  
Chalmers University of Technology  
Gothenburg, Sweden 2013

Spectroscopic Studies of Biomolecules Confined in Self-Assembled Nanostructures  
NILS CARLSSON

ISBN 978-91-7385-885-4

© NILS CARLSSON, 2013.

Doktorsavhandlingar vid Chalmers tekniska högskola

Ny serie nr: 3566

ISSN 0346-718X

Department of Chemical and Biological Engineering

Chalmers University of Technology

SE-412 96 Gothenburg

Sweden

Telephone + 46 (0)31-772 1000

Cover:

Schematic illustration of left: a mesoporous particle and the hexagonal pore symmetry and right: The periodic minimal surface representing the diamond cubic phase symmetry of a lyotropic liquid crystal.

Printed by Chalmers Reproservice

Gothenburg, Sweden 2013

# SPECTROSCOPIC STUDIES OF BIOMOLECULES CONFINED IN SELF-ASSEMBLED NANOSTRUCTURES

Nils Carlsson

Department of Chemical and Biological Engineering  
Chalmers University of Technology

## Abstract

The present thesis examines the effects of incorporating biomolecules into self-assembled nanostructures. This approach is exemplified by short DNA molecules in environments close to lipid bilayers and the immobilization of enzymes into mesoporous silica particles. The biomolecules and attached chromophore probes are studied in the nanostructures using optical spectroscopy. An important part of the thesis work is the spectroscopical considerations enforced by the complex samples formed by the biomolecules and the nanostructures. The small confining spaces rich in surfaces have effects on the physical properties of the nanostructures.

The movement of the large biomolecules are hindered by the narrow environments and this is utilized for electrophoretic separation and orientation of oligonucleotides in lyotropic liquid crystals. The cubic phase of the monoolein-water system was shown to act as an electrophoresis matrix for both water soluble oligonucleotides and bilayer anchored molecules. The lamellar phase of the sodium octanoate-decanol-water system was used to introduce macroscopic ordering of oligonucleotides and bilayer bound chromophores for studies by linear dichroism. In addition to the orientational effects of the chromophores interacting with the lipid bilayers, spectral effects of the bilayer environment were also studied.

In the spectroscopic studies of enzyme immobilized into mesoporous silica particles the pore pH were found to be slightly different compared to the external volume. Furthermore, direct spectroscopic determination of the pore loading was examined in contrast to common indirect approaches. Finally, the concept of pore filling as an analysis tool and the particle size influence on immobilization are discussed.

# List of Publications

The thesis is based on the work contained in the following articles, referred to by Roman numerals in the text:

- I Nils Carlsson, Ann-Sofie Winge, Sven Engström and Björn Åkerman\*  
Diamond cubic phase of monoolein and water as an amphiphilic matrix for electrophoresis of oligonucleotides  
*Journal of Physical Chemistry B*, 2005, 109, 18628-18636.
- II Nils Carlsson, Nima Sanandaji, Marina Voinova, and Björn Åkerman\*  
Bicontinuous cubic phase of monoolein and water as medium for electrophoresis of both membrane-bound probes and DNA  
*Langmuir*, 2006, 22, 4408-4414.
- III Nils Carlsson\*, Fabian Jonsson, L. Marcus Wilhelmsson, Bengt Nordén, and Björn Åkerman  
DNA hosted and aligned in aqueous interstices of a lamellar liquid crystal – a membrane-biomacromolecule interaction model system  
*Soft Matter*, 2013, 9, 7951-7959
- IV Fredrik Westerlund, Jonas Elm, Jacob Lykkebo, Nils Carlsson, Erling Thyrhaug, Björn Åkerman, Thomas Just Sørensen, Kurt V. Mikkelsen, and Bo W. Laursen\*  
Direct probing of ion pair formation using a symmetric triangulenium dye  
*Photochemical and Photobiological Sciences*, 2011, 10, 1963-1973.
- V Maria Matson, Nils Carlsson, Tamás Beke-Somfai, and Bengt Nordén\*  
Spectral properties and orientation of voltage-sensitive dyes in lipid membranes  
*Langmuir*, 2011, 28, 10808-10817.
- VI Christian Thörn, Nils Carlsson, Hanna Gustafsson, Krister Holmberg, Björn Åkerman\*, Lisbeth Olsson  
A method to measure pH inside mesoporous particles using protein-bound SNARF1 fluorescent probe.  
*Microporous and Mesoporous Materials*, 2013, 165: p. 240-246.
- VII Nils Carlsson, Hanna Gustafsson, Krister Holmberg, Björn Åkerman  
Determination of immobilized protein content in mesoporous particles  
*Manuscript*
- VIII Nils Carlsson†, Hanna Gustafsson†, Christian Thörn†, Lisbeth Olsson, Krister Holmberg\*, and Björn Åkerman  
Enzymes immobilized in mesoporous silica: a physical-chemical perspective  
*Submitted to Advances in Colloid and Interface Science*

# Contribution Report

- Paper I: Mainly responsible for performing experiments and analysis.
- Paper II: Mainly responsible for performing experiments and analysis.
- Paper III: Mainly responsible for performing experiments, analysis, and writing the paper.
- Paper IV: Performed experiments, analysis and writing of the part on orientation in liquid crystals.
- Paper V: Performed experiments and analysed data together with MM. Wrote parts of the paper.
- Paper VI: Performed experiments and analysed data together with CT. Wrote parts of the paper.
- Paper VII: Mainly responsible for performing experiments, analysis, and writing the paper
- Paper VIII: Wrote the paper together with CT and HG

## Publications not included in this thesis

The following publications by the author are not included in this thesis.

- IX Nima Sanandaji, Nils Carlsson, Marina Voinova, and Björn Åkerman\*  
Comparison of oligonucleotide migration in a bicontinuous cubic phase of monoolein and water and in a fibrous agarose hydrogel  
*Electrophoresis*, 2006, 27, 3007-3017.
- X Nils Carlsson\*, Annika Borde, Sebastian Wölfel, Björn Åkerman, and Anette Larsson  
Quantification of protein concentration by the Bradford method in the presence of pharmaceutical polymers.  
*Analytical Biochemistry*, 2011, 411(1): p. 116-121.
- XI Nils Carlsson\*, Catherine C. Kitts, and Björn Åkerman  
Spectroscopic characterization of Coomassie Blue and its binding to amyloid fibrils  
*Analytical Biochemistry*, 2012, 420(1): p. 33-40.
- XII Hanna A. Rydberg, Nils Carlsson, and Bengt Nordén\*  
Membrane interaction and secondary structure of *de novo* designed arginine and tryptophan peptides with dual function  
*Biochemical and Biophysical Research Communications*, 2012, 427, 261-265.

# Table of Contents

1	Introduction .....	1
2	Lipid membranes .....	3
2.1	Amphiphiles .....	3
2.2	Amphiphilic aggregates .....	3
2.3	Lyotropic liquid crystals .....	5
2.4	Additional lipid structures .....	7
2.5	Biological membranes .....	8
2.6	Model membranes .....	9
3	Enzyme immobilization in mesoporous particles .....	11
3.1	Immobilization benefits .....	11
3.2	Materials .....	11
3.3	Immobilization studies .....	12
4	Photophysics .....	15
4.1	Light properties .....	15
4.2	Light – matter interaction events .....	16
4.2.1	Excitation .....	16
4.2.2	Relaxation of the excited state .....	18
4.2.3	Scattering of light .....	20
5	Analytical techniques .....	23
5.1	Spectroscopic techniques .....	23
5.1.1	Absorption spectroscopy .....	23
5.1.2	Fluorescence spectroscopy .....	28
5.1.3	Linear dichroism .....	30
5.2	Standard protein assays .....	31
5.2.1	Intrinsic protein absorbance assays .....	32
5.2.2	Extrinsic absorbance assays .....	33
5.2.3	Extrinsic fluorescence assays .....	34
5.3	Electrophoresis .....	35
6	Applications of liquid crystals .....	37
6.1	Electrophoretic migration in a cubic phase .....	37
6.2	Orientation of short oligonucleotides .....	39
6.3	Dye – bilayer interaction .....	42
6.3.1	Position and orientation of dyes .....	42
6.3.2	Spectral effects of solvents and bilayer interaction .....	47
7	Spectroscopic studies of immobilized enzyme .....	49
7.1	Spectroscopic effects of particle suspensions .....	49
7.2	Direct pore loading determination .....	51

7.3	Pore filling analysis.....	53
7.4	Pore pH and pore microenvironment.....	55
8	Concluding remarks.....	58
9	Acknowledgements.....	60
10	References.....	61



# I Introduction

A nanostructure has one or more dimensions on the nanometre scale, *i.e.* below 100 nm. To be considered a nanostructure it should show regularity on the nanometre scale or be at least partly arranged or synthesized by design at that level [1]. A key objective in using nanostructures is that they have different physical properties that are especially interesting at the nanometre scale. Especially in connection to studies of biomolecules it should be noted that many of the complex biological structures are on this scale and biomolecule properties may be different when studied in bulk solution. The materials used in this thesis all have periodic structures on the sub ten nanometre scale, namely lipid bilayers or silica surfaces. Two different approaches are used for producing nanostructures: A bottom-up approach building nanometre sized structures from molecules and a top-down approach using microfabrication methods such as lithography to shape a larger object in a nanometre sized way. The bottom-up approach relies on the chemical properties of the components to self-assemble into a useful conformation [2]. The limitations for both approaches are size, but in opposite ways. The resolution of top-down techniques limits the formation of the smallest objects, while complexity limits the bottom-up fabrication of larger objects. The periodic structures in this thesis are small to be top-down manufactured with today's standard techniques and further the 3D character is even harder to produce in that manner. Instead the nanostructures are self-assembling soft lipid structures or solid silica structures made with soft self-assembled templates.

The first part of the results in this thesis (section 6) concerns the incorporation of biomolecules and optical spectroscopy probes into a lipid rich environment. The environments studied are high concentration lipid constructs that self-assemble in water, so called lyotropic liquid crystals. The lipids form bilayers that can be seen as models of the biological membrane structures. The incorporation of biomolecules into this environment may affect both the biophysical properties and also the spectroscopical properties of the probes. The liquid crystals are used both for their structural properties with nanometre sized compartments and for their model membrane capacity. The structural properties are used in papers I-III to separate or orient short DNA molecules. The polar/apolar character of bilayers is a property utilized in papers III-V.

The second part of the results (section 7) concerns incorporation of enzymes into solid, porous particles of silica creating a biocatalytic material. The particles are

made using liquid crystals as a template and the nanometre size of the pores are similar to the distances between the lipid bilayers in the lyotropic liquid crystals used in section 6. The properties of the silica particles can be tailor made (section 3.2) to suit the enzyme application and can be seen to enhance several useful properties of the enzyme such as the product selectivity as further developed in section 3.1 and paper VIII. Spectroscopic studies were used to study the amount of enzyme immobilized in paper VII and the pH of the pore environment in paper VI.

The common themes in this thesis are how biophysical properties are affected by the confinement by different nanostructures and the spectroscopical challenges of studying these complex samples consisting of different environments. Especially in these cases it is important to determine the character of the signals and separate the components. It is also important to validate the measurement technique to know the origin of the signal. The results of the research contained in this thesis are discussed in sections 6 and 7. Before the results an overview of lipid membranes (section 2), enzyme immobilization into mesoporous particles (section 3), photophysics (section 4) and the analytic techniques used (section 5) is given.

## 2 Lipid membranes

### 2.1 Amphiphiles

Depending on the electronic characteristic of a molecule it may be soluble primarily in polar or non-polar solvents. Those molecules soluble in polar solvents are generally referred to as hydrophilic (water loving, from Greek) and their opposites as hydrophobic. Molecules of mixed character are often found to have solubility between the two extremes. Molecules containing separated domains with hydrophilic and hydrophobic properties respectively are called amphiphilic. These amphiphilic molecules are often found at the surface between solvents of different polarity, such as oil-water but also air-water, arranged with the hydrophilic part in the polar solvent and *vice versa*. This behaviour has rendered this class of molecules the name surfactants, which is short for surface active agents. Surfactants are commonly used as for their cleaning properties in detergents and soaps and as emulsifiers facilitating and stabilizing mixtures of oil and water.

Surfactant molecules commonly have a long hydrophobic “tail” part of hydrocarbons and a polar “head”-group that is either ionic or non-ionic, *e.g.* hydroxyl groups. When dispersed at low concentration in water there will be both unimers (single molecules) dissolved in the bulk of the solvent and enrichment at the surface, minimizing the interaction energy between the polar solvent and the non-polar tails. Other solvents than water are left out of this section, but surfactants in other polar solvents behave similarly and in non-polar in the opposite way [3]. Raising the concentration will eventually fill the surface with surfactant molecules. At this point aggregates will start to form in the solution [4-7], and further addition of surfactants will be in the form of these aggregates called micelles [8, 9]. The concentration where micelles (Figure 1) start to form is called the critical micelle concentration (CMC).

### 2.2 Amphiphilic aggregates

The shape of molecular aggregates formed by surfactants depends on the size of the different parts of the surfactant molecule. Repulsive forces between the head-groups and attractive hydrophobic interfacial forces determine the optimal equilibrium head-group area,  $a_e$ . The tail volume,  $V_o$ , and the critical chain length,  $l_o$ , sets limits on how the molecules can pack themselves in an aggregate. These geometrical packing conditions define the dimensionless shape factor, or packing

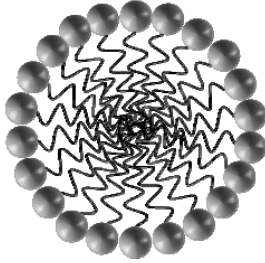


Figure 1 Schematic cut-through picture of a micelle. As an example, the common surfactant SDS has a CMC of  $8 \mu\text{m}$  (at  $25^\circ\text{C}$ ) and an aggregation number of about 60 in water.

$$P = \frac{V_0}{a_e l_0} \quad (1)$$

parameter,  $P$  (equation 1 [10]), which is expected to determine the structures formed (Table 1).

When forming a micelle (Figure 1) the surfactants arrange themselves in a spherical shape with the polar head-groups facing the water and the hydrophobic tails towards the centre of the micelle. The number of molecules that form a micelle, the aggregation number, varies between molecules, but also from *e.g.* temperature. The size of micelles is fairly independent of surfactant concentration. By changing *e.g.* salt concentration the surfactants can form other micelle shapes such as rods. When reaching very high concentrations of surfactants the free space in the solution becomes limited. The micelles then arrange to minimize contact between themselves resulting in a micelle close-packing, a micellar cubic phase [11, 12]. This structure and

Table 1 Packing parameter<sup>1</sup> of amphiphilic molecules.

Packing parameter	Critical packing shape	Structures formed
$<1/3$	Cone	Spherical micelles
$1/3-1/2$	Truncated cone	Cylindrical micelles
$1/2-1$	Truncated cone	Flexible bilayers, vesicles
$\sim 1$	Cylinder	Planar bilayers
$>1$	Inverted truncated cone	Inverted micelles

1. See equation 1

the ones described below are called lyotropic liquid crystals, since they are molecularly disordered in a liquid fashion, but have a long-range crystal order.

## 2.3 Lyotropic liquid crystals

At even higher concentrations there is no longer room for separate micellar structures and larger liquid crystal structures are formed. These liquid crystals can be continuous in one, two or three dimensions. The one-dimensional structures can be seen as long tubular micelle structures arranged in hexagonal symmetry in a continuous water domain (hexagonal phase) [11, 13] as seen in Figure 2A. They can also have the direction of the surfactants reversed forming separate water channels in a continuous hydrophobic domain (inverted hexagonal phase). The surfactants can also form bilayer structures, *i.e.* two-layer sheets with the hydrophobic tails towards the centre of the sheet and the hydrophilic head-groups exposed to the water. By stacking these bilayers parallel to each other a two-dimensional liquid crystal shown in Figure 2B is formed (lamellar phase) [14, 15]. Both the bilayers and the aqueous interstitia respectively are continuous in two dimensions. The thickness of the water interstitia in between the parallel bilayers of the lamellar liquid crystal has been found to be fairly uniform [13]. The cubic phases consist of curved infinite bilayers and exhibit periodicity in all three dimensions. The liquid crystalline phases described above are in phase diagrams often denoted:  $I_1$  and  $I_2$ , micellar cubic,  $I_\infty$ , lamellar,  $H_1$ , hexagonal, and  $H_2$ , inverted hexagonal, respectively [16]. The subscript number reflects on the character of the dispersed phase and the dispersion medium. The phases denoted  $X_1$  are oil-in-water phases and the  $X_2$  phases are water-in oil.

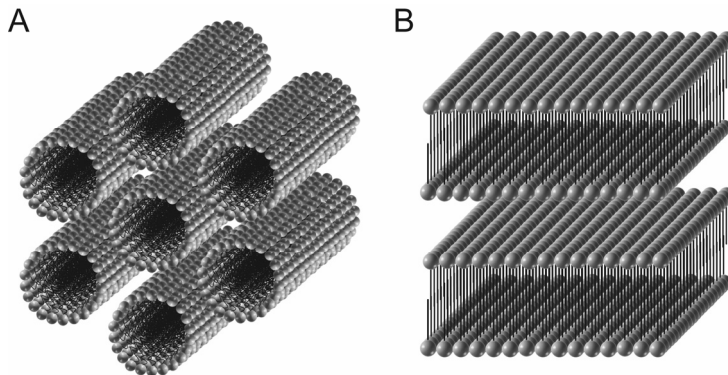


Figure 2 Schematic illustrations of lyotropic liquid crystals of A. hexagonal and B. lamellar symmetry.

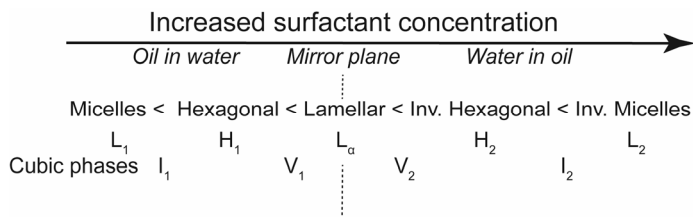


Figure 3 The Fontell Scheme [12] for the ideal order of the liquid crystalline phases as a function of the surfactant concentration.

The bicontinuous cubic phases are sometimes denoted  $V_1$  and  $V_2$ , respectively. This notation describes the character but not the shapes and geometry of the cubic phases as will be elaborated on below. The concentration dependence of the liquid phases of an ideal surfactant can be seen in Figure 3.

An important tool for understanding the shapes of the cubic phase bilayers is the periodic minimal surfaces [17]. In mathematics the minimal surface is a surface that minimizes its area within some constraints. This type of mathematical problems can be demonstrated by the use of a soap film minimizing the energy for forming film surfaces. A minimal surface can also exhibit crystallographic periodicity and is then called an infinite periodic minimal surface, IPMS. There are several cubic phases with different geometries that can be described by periodic minimal surfaces with their geometries shown in Figure 4. All three consist of two separated continuous channel systems and one continuous surface. In lyotropic liquid crystals the channel systems are filled with water and the surface is a lipid bilayer [12, 18]. The simplest geometry of the cubic phases is described by primitive periodic minimal surface (P), derived by Schwartz [17]. The unit cell has three orthogonal channels, which are connected to the adjacent unit cells forming a cubic array (Figure 4). This structure is represented in crystallography by the space group  $Im\bar{3}m$  or  $Q^{229}$ . This crystallographic notation is

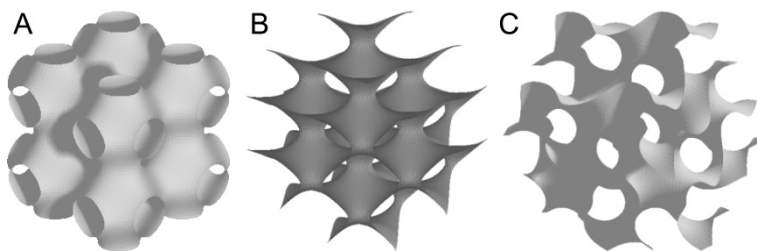


Figure 4 Periodic minimal surfaces representing the geometries of cubic phases. The corresponding cubic phases have bilayers centred on the minimal surface. The cubic phases are from the left: Primitive (P), diamond (D), and gyroid (G). The surfaces are drawn using the functions defined in [19]

often used in lyotropic liquid crystal phase diagrams. The diamond (D) surface, also derived by Schwartz [17], is represented by the space group Pn3m or Q<sup>224</sup>. In this structure the bilayer and the two channel systems are arranged to form a diamond lattice (Figure 4). The gyroid (G) surface, derived by Schoen [20, 21], is represented by the Ia3d or Q<sup>230</sup> space group. The aqueous channels of the G-cubic phase are helical, one left-handed and the other right handed, and extending through the matrix. These three structures are related so one of them can be continuously deformed into another. G is an intermediate form when deforming from P to D. For a thorough exploration of the mathematical field of minimal surfaces see [22].

A minimal surface is as convex as it is concave in all points and hence, the mean curvature is zero. For a bilayer situated around a minimal surface the averaged Gaussian curvature,  $\langle K \rangle$ , is smaller than or equal to zero everywhere. The packing parameter for such a structure is related to the averaged Gaussian curvature according to equation 2 [23]:

$$P = \frac{1 + \langle K \rangle l^2 / 3}{1 + \langle K \rangle l^2} \quad (2)$$

Consequently the packing parameter must be equal to or larger than one for obtaining such a cubic structure. An increase in the packing parameter results in a decrease in the averaged Gaussian curvature. The larger the value of  $K$ , the flatter the surface, *e.g.* a flat structure like a planar bilayer has a shape factor of about one and an averaged Gaussian curvature of about zero. The different cubic phases correspond to different packing parameters and thereby to different averaged Gaussian curvatures. The packing parameter of the P-phase is smaller than the packing parameter of the D-phase and therefore the P-phase forms a flatter surface [24].

## 2.4 Additional lipid structures

The descriptions above for structures formed by surfactants are in many cases also applicable for solutions of polymers composed of blocks of different polymerized monomers, so called block copolymers. There are examples of block copolymers consisting of poly(ethylene glycol)-poly(propylene glycol)-poly(ethylene glycol) that form liquid crystalline structures with hexagonal symmetry. These liquid crystals have found applications as templates for synthesis of porous particles [25, 26] and as electrophoresis separation matrix [27, 28]. Both these applications will be further discussed below (sections 3.2 and 6.1).

Thermodynamically stable irregular phases such as microemulsions ( $L_1$ ,  $L_2$ ) [16, 29] and sponge ( $L_3$ ) [16, 30] can also be used for studies of biomolecules but are not further described here. There are some thermodynamically unstable bilayer structures resembling biological structures that are commonly used as biophysical model membranes. A vesicle is a bilayer structure enclosing an inner volume [31]. Vesicles with a single bilayer are called unilamellar and if there are several parallel bilayers enclosing the inner volume the vesicles are called oligolamellar. A multilamellar vesicle has its whole volume filled with homocentric bilayers. Continuous planar membranes can be made on a solid support, so called supported bilayers [32]. These supported bilayers *e.g.* make membrane structures available for study by surface sensitive analytical techniques [33].

In the phase diagram the liquid crystalline phases are found above the Krafft temperature [12], which varies with system composition. For bilayers this temperature is also referred to as the transition temperature. For each sample, above this temperature the hydrocarbon tails of the lipids are in a fluid state, while they are more ordered at a lower temperature in either a gel ( $L_\beta$ ,  $L'_\beta$ ,  $P_\beta$ ) or a crystalline state ( $L_c$ ) [34]. The prime indicates that the lipid tails are tilted relative to the bilayer normal. Vesicles and supported bilayers can be in either the fluid or in the gel state depending on composition and temperature. In bilayers of mixed composition there is a possibility that the lipids separate in domains of different state that can coexist in the same bilayer [35, 36]. The transition temperature is lower for lipids with unsaturated tails than for those with saturated tails and the position of the unsaturated bond influences the melting temperature [34]. It is also higher for longer tails than for shorter tails of the same saturation [37]. Head group interactions have also been seen to affect the transition temperature in bilayers [38] and some transitions are sensitive to bilayer stress [39]. The bending rigidity of the membrane increases steadily with increasing tail length for saturated and mono-unsaturated lipid chains [40]. Poly-unsaturated chain bilayers (more common in brain tissue) are thinner and more flexible than bilayers with saturated and mono-unsaturated tails that dominate common animal cell membranes.

## 2.5 Biological membranes

The cell membrane separates the interior of the cell from the outside environment providing a barrier against diffusive transport. Other membrane structures provide compartmentalization of the cell. Bilayer structures are found in the organelle membranes including *e.g.* nucleus, mitochondria, and endosomes. There are further the endoplasmic reticulum and the Golgi apparatus, organelles mainly

built by membrane rich structures. All these cellular membrane structures are built by amphiphilic molecules, in this context often called lipids. Several classes of lipids are found in biological membranes such as phospholipids and glycolipids both with saturated and unsaturated fatty acid chains. In addition the membrane consists of up to 50% surface bound and transmembrane proteins in weight. The proteins can be seen as freely moving in the bilayer membrane in the fluid mosaic model [41]. This model views the cell membrane as a two-dimensional solution of oriented lipids and proteins alternating, with the lipids as the matrix. Many important functions are performed by the lipid membrane in cooperation with the membrane proteins, where signal transmission is a viable example.

Biological configurations like the endoplasmic reticulum and the Golgi apparatus have cubic lipid nanostructures that resemble the cubic phases [42, 43]. These structures also have an important part in the function of these organelles. Cubic structures can also be found in other lipid rich organelles such as pre-chloroplasts [44]. In the digestion of fat cubic phases are directly involved in the transport mechanism [44].

## 2.6 Model membranes

For many biophysical studies the biological cell is too complex. The membrane properties are often studied using a less complex model *e.g.* without the large protein content. The earliest bilayer model membrane is known as black lipid membranes [45]. The membrane bilayer is formed to span a hole in a solid support. With black lipid membranes both sides of the membrane are accessible and can be modified individually. This makes them useful for electrical characterization *e.g.* of voltage gated ion channels [46], with one electrode at each side of the membrane. A supported lipid membrane [32] is a planar bilayer sitting on a solid support. Unlike black lipid membranes, only one side of the bilayer is exposed to the bulk solution with only a thin hydration layer between the other side of the bilayer and the solid support. The supported lipid membranes are suited for use with techniques based on detection of properties near to a surface such as quartz crystal microbalance [47], total internal reflection fluorescence microscopy [48] and surface plasmon resonance [49]. Supported lipid membranes are much more stable than the black lipid membrane allowing for long experiments.

Mixtures of short and long tailed lipids may spontaneously form discrete flat bilayer structures with the shorter lipids forming the edges and the longer lipids the bilayer of these bicelles [50]. These structures can be oriented by a magnetic field [51]

and have therefore been used for solid state nuclear magnetic resonance studies of bilayers and *e.g.* membrane proteins [52]. Recently, these bicelles were found to align also in a shear flow in a polarized light study [53]. Vesicles [31] can be formed by various lipid compositions tailoring surface charge and bilayer order. The concentration of vesicles as well as their size can be varied within wide ranges. One feature of vesicles is that they have an interior volume and transport in and out can be studied. Vesicles are often used for bulk measurements and with optical techniques. Liquid crystals as model membranes [54, 55] provide high area of membrane per unit volume that can be utilized to achieve the required optical density for some optical spectroscopy techniques as in papers III-V. They are also used as model system for the stacked membrane structures formed in organelles such as the endoplasmic reticulum and the Golgi apparatus due to the structural relevance of the three dimensionally organized bilayers [43].

The probability of finding different characteristic parts of the lipid molecules and other guest molecules, such as water, strongly depends on the distance from the bilayer centre [56]. For phospholipids water can penetrate the bilayer in to the glycerol backbone of the lipids. This radial polarity profile is important for the location of guest molecules in the lipid bilayer. It is also important to note that addition of guest molecules to the model membranes may change *e.g.* their phase behaviour [57]. This can then change the basis for the use of some analytical techniques. On the other hand this change in the membrane properties may be a central part in the biological effect of these guest molecules [58]. Incorporation of a single transmembrane protein may disturb an ordered bilayer phase [59].

## 3 Enzyme immobilization in mesoporous particles

### 3.1 Immobilization benefits

Enzyme immobilization for biocatalytic applications is generally used to improve the protein stability and enzymatic function as well as for easy recovery of both product and enzyme [60]. The interest in mesoporous materials is broad as their applications involve controlled drug release and recently targeted cancer therapies [61, 62] and as immobilization support they have some unique advantages. The porous structure allows for high enzyme loadings and creates a protective environment where the enzymes can withstand elevated temperature, higher salt concentrations, and more extreme pH [60, 63]. The pore diameter can be tuned to match the size of the targeted enzyme and the possibility of silica surface modifications may be used to enhance or direct the enzyme activity. Interestingly, the confinement of enzymes into the pores can affect both the specific activity and the substrate selectivity of the immobilized enzymes.

Based on electrostatic and hydrophobic interactions, strategies for rational design of mesoporous materials for enzyme immobilization have been proposed [64]. In this model the properties of the proteins and particles are somewhat treated as separate entities which acknowledges but does not include the possibility that the pore environment may affect the properties of the proteins. In paper VIII we review the analytical techniques used in studying immobilization of enzymes in mesoporous silica. Techniques both for studying interaction between silica and proteins but also for studying the immobilization process and enzyme activity are discussed.

### 3.2 Materials

A mesoporous material is defined as containing pores with diameters between 2 and 50 nm [65]. Materials with pores with diameters of less than 2 nm are referred to as microporous and when the pores have diameters larger than 50 nm the material is macroporous. Mesoporous, solid particles with regular symmetry can be synthesized using a liquid crystal as a template. This thesis will focus on particles made by silica, but there are similar porous structures in other metal oxides [66] *e.g.* alumina [67, 68] and titania [69] synthesized for numerous applications [70]. There are silica particles with the pores arranged in both hexagonal symmetry, *e.g.* SBA-15 [25, 26] and MCM-41 [71, 72], as well as cubic symmetry, *e.g.* SBA-16 [26] and MCM-48 [73], made using

either liquid crystal forming surfactants [71-73] or block co-polymers [25, 26] as a template. In addition to the structured symmetrical materials various disordered structures are available.

In short, the particles are synthesized by mixing the block co-polymer, or surfactant, with the silica precursor in an aqueous solution. The precursor is hydrolyzed and polymerizes in the water domain of the template liquid crystal, forming an inorganic network mirroring the template structure. After the polymerization reaction the formed silica material can be hydrothermally treated for increased cross-linking, tuning of the pore diameter, and particle growth. Finally, the amphiphilic template is removed by calcination or extraction, resulting in a solid mesoporous material.

A combination of analytical techniques is commonly used to characterize the properties of the mesoporous material [25, 72, 74, 75]. X-ray diffraction [76] can be used to determine the structural symmetry of the material. As a complement to X-ray diffraction transmission electron microscopy can be used to determine the local pore structure. The particle size and morphology can be visualized using scanning electron microscopy [77]. Nitrogen physisorption analysis can be used to determine the surface area, pore volume and the pore size distribution [78]. The adsorbed amount can be determined using the ideal gas law and the BET gas adsorption method [79].

The surface of mesoporous silica is rich in silanol (SiOH) groups that can be used for organic functionalization [80]. The functionalization could either be used for tuning the surface properties by surface modification or for adding a specific function to the particle. This is used for designing sensors [81] for *e.g.* detecting vapour [82] or pH [83]. By performing different modifications before and after removing the amphiphilic template the pore surface could be modified in one way and the particle outer surface in another [84].

### 3.3 Immobilization studies

Enzymes can be immobilized into mesoporous silica particles either by covalently attaching to the support material or passively by physical adsorption and electrostatic interaction between the enzyme and the surface. For covalent attachment typically the surface is modified by functionalizing the silanol groups on the surface. One procedure is to first attach an amino-silane compound to the surface and then add a cross-linking agent. Finally the enzyme is added and covalently bound to its amino groups [85]. Physical adsorption involves weak forces between the enzyme and the surface. This interaction can be improved if there is electrostatic

attraction between the enzyme and the silica surface (and inversely with electrostatic repulsion). In searching for ideal immobilization conditions changing the pH may increase the electrostatic attraction. Depending on the isoelectric point of the enzyme surface either modifying the silica support (pI  $\sim$  2) or replacing it with either titania (pI  $\sim$  5) or alumina (pI  $\sim$  8) may be beneficial [86]. In studying the pH effect on immobilization and on the immobilized enzymes [87-89] questions about the pore environment were raised and later studied in paper VI.

Here some of the common parameters studied in enzyme immobilization will be described. There is some term ambiguity in the field of enzyme immobilization as discussed in paper VIII that is not further elaborated on here. The adsorption isotherm describes the amount of a solute that adsorbs at a surface as a function of the solution concentration. The equilibrium amounts are determined for each fixed enzyme concentration while keeping the temperature constant. The adsorption isotherm can be used to determine how much of the enzyme can be immobilized into a given material. If a lower enzyme loading is desired this can be achieved by adjusting the enzyme concentration accordingly. By observing how the adsorbed amount develops over time one can determine the adsorption rate. This is useful to determine the amount of time needed for the immobilization process. The adsorbed amount is commonly estimated using indirect techniques which have poor time resolution. The use of direct monitoring of the adsorption in real-time could provide more detailed information required to test models of the immobilization process as discussed further in paper VIII and briefly in section 9. The effect on the enzyme activity by immobilization can be estimated by the immobilization efficiency. Here the specific activity of the immobilized enzyme is compared to the specific activity of free enzyme. An enhanced activity yields immobilization efficiency over 1 and lowered activity consequently a value below 1.

In enzyme immobilization applications described above the amount of protein present has to be known for the design and evaluation of the systems. This is also applicable for monitoring of loading of and leakage from particles. See below for section 5.2 on standard protein assays. This issue is further discussed in terms of direct and indirect measurements in paper VII and in section 7.2.

There are some techniques that have been employed to visualize the enzymes in the mesoporous particles. One setup is by using transmission electron microscopy on slices of the particles. The enzyme location is shown by immunogold staining *i.e.* colloidal gold particles visible in electron microscopy are attached to secondary antibodies binding to primary antibodies binding to the enzyme of interest [90].

Fluorescence microscopy was used to show the immobilization of an immobilized protein [91] and the location of the immobilized protein. It has also been used to study two co-immobilized enzymes showing their respective location in the particles [92]. Fluorescence microscopy including an energy transfer setup between different fluorescent proteins that were co-immobilized using FRET (section 5.1.2) [93, 94] were used to illustrate the possibility of immobilization of different enzymes in the same pore. There are examples of images showing enzyme filling the entire volume of the particle as well as an increased concentration near the pore openings. Some further aspects on the pore filling will be discussed in section 7.3.

## 4 Photophysics

Photophysics describes the physics of light, especially the interaction between light and matter. This chapter is divided in two sections concerning light and light-matter interactions.

### 4.1 Light properties

Light is electromagnetic radiation, but not all electromagnetic radiation is generally referred to as light. Electromagnetic radiation comprises of high energy radiation such as gamma-rays and X-rays as well as low energy microwaves and radio waves. Between these in energy are the infrared, the visible light and the ultraviolet. Although visible light (400-700 nm) is the only light we can see by eye it is common to include also near-infrared (NIR), near and middle ultraviolet when discussing light in a spectroscopic perspective. The energy of light is described by equation 3

$$E = hf = hc\tilde{\nu} = \frac{hc}{\lambda} \quad (3)$$

where  $h$  the Planck constant,  $f$  is the frequency,  $\tilde{\nu}$  is the wavenumber,  $c$  is the speed of light in vacuum, and  $\lambda$  is the wavelength. These different measures are normally used by chemists and physicists to describe the energy of electromagnetic radiation and particularly light in different scientific disciplines. The units used are commonly  $\text{cm}^{-1}$  for wavenumber, Hz for frequency and nm for wavelength. Throughout this thesis these measures will be applied more or less in the common use. Furthermore, to be able to describe the properties of light many physicists agree that it can be described both as waves and as particles (photons), the so called wave particle duality that also applies to all matter [95]. In this thesis the many of the light characteristics will be described as wave properties, while in some of the interaction events the photon notation will be used.

The electromagnetic radiation is characterized by an electric field  $\mathbf{E}$  and a magnetic field  $\mathbf{B}$  that are oscillating orthogonal to each other and both perpendicular to the propagation direction. The radiation may be described as a transverse wave perpendicular to the propagation direction. The polarization of this wave is defined by the direction of the electric field of the wave, and accordingly, perpendicular to the propagation. The electric field vector  $\mathbf{E}$  may be divided in two perpendicular components in an arbitrary coordinate system where the two components are

oriented along the x and y axis respectively with z indicating the direction of propagation. The two sinusoidal components may differ in both amplitude, and phase according to equation 4 [96]

$$\begin{cases} E_x = a_x \cos(kz - \omega t) \\ E_y = a_y \cos(kz - \omega t + \delta) \\ E_z = 0 \end{cases} \quad (4)$$

where  $a$  is the amplitude,  $k=2\pi/\lambda$  is the wave constant,  $\omega=kv$  is the circular frequency and  $\delta$  is the phase difference. The expression within the cosine brackets is called the phase. The wave is linearly polarized if the vectors are in phase or 180 degrees out of phase. In equation 4 this is represented with the phase difference being either zero or a multiple of  $\pm\pi$  (*i.e.*  $\delta=n\pi$  and  $n=0, \pm 1, \pm 2 \dots$ ). The projection on the xy plane with time will be produce straight line. Circular polarization is achieved when the two vectors first have equal amplitude second have the two vectors 90 degrees out of phase. The projection on the xy plane rotates with time either clockwise (right-circularly polarized) or counter-clockwise (left-circularly polarized). In equation 4 the right-circularly polarized light is represented by  $\delta=-\pi/2+2n\pi$  and the left-circularly polarized light by  $\delta=\pi/2+2n\pi$  (in both cases  $n=\pm 1, \pm 2 \dots$ ). Any other phase difference will produce an elliptic xy projection. Natural light has a random polarization where the light is composed of all polarization states.

## 4.2 Light – matter interaction events

The light-matter interactions discussed in this part are interactions between light (as described above) and molecules or particles.

### 4.2.1 Excitation

Absorption is when the energy of a photon is taken up by matter; for visible light typically by an electron in a molecule. For this process to be possible the energy of the photon should match the energy gap to a higher electronic level of the electron. This condition is described in equation 5 and is known as the Bohr frequency condition [97].

$$\Delta E = \frac{hc}{\lambda} \quad (5)$$

The quantized electronic states of molecules as well as the transition between them can be illustrated by a Jablonski diagram [98] (Figure 5). For atoms this condition

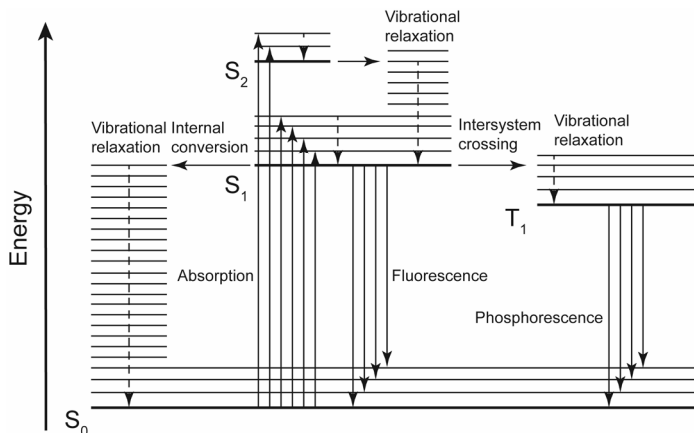


Figure 5 Jablonski diagram showing electronic transitions in molecules. Radiative transitions are shown by solid vertical arrows while non-radiative transitions between electronic states are represented by horizontal solid arrows. Non-radiative lowering of energy by vibrational relaxation is represented by dashed arrows. Electronic states are shown by thick lines and vibrational sub-states by thinner lines.

results in narrow absorption intervals, but for molecules the available vibrational energy levels provide possibilities for absorption of wider ranges of light by one transition dipole moment. The transition dipole moment is the electric dipole moment associated with the transition between two electron configurations in the molecule. It can be seen as a vector with a fixed position within the molecule. The transition moment dipole vector,  $\mu$ , is described in equation 6

$$\mu_{i \rightarrow f} = \langle \Psi_f | \hat{\mu} | \Psi_i \rangle \quad (6)$$

where  $\Psi$  represents the wave functions of the initial and final stages, respectively, and  $\hat{\mu}$  is the electric dipole moment operator. The probability,  $P$ , of an absorption event to occur depends on the angle,  $\theta$ , between the transition dipole moment and the electronic vector of the light (equation 7).

$$P \propto |\mu_{i \rightarrow f}|^2 \cos^2 \theta \quad (7)$$

A molecular electronic singlet state has all electron spins paired. In a singlet excited state the spin of the excited electron is still paired with the lone ground state electron. In a triplet excited state the two electrons are no longer spin paired. The ground state is in most molecules a singlet state denoted  $S_0$ . The singlet excited states are denoted  $S_n$  ( $n=1, 2, \dots$ ) and correspondingly the triplet excited states  $T_n$  ( $n=1, 2, \dots$ ). Almost

all excitation events occur between  $S_0$  and a higher singlet state  $S_n$ . These notations are used to show different electronic states in Figure 5.

### 4.2.2 Relaxation of the excited state

The excited state is fairly unstable and the molecule will eventually return to the ground state. The relaxation from the excited state may occur in steps either radiatively (light is emitted) or non-radiatively. There are several pathways for this relaxation shown in Figure 5. Starting with the main focus of this work; fluorescence is a radiative relaxation from  $S_n$  to  $S_0$ . In general the relaxation is between  $S_1$  and  $S_0$  regardless of which singlet excited state the molecule was excited to [99]. For any molecular bond, the individual atoms are confined to specific vibrational modes, in which the vibrational energy levels are quantized in a manner similar to electronic energies (thin lines in Figure 5). The energy difference between a  $S_0$  to  $S_1$  excitation and a  $S_1$  to  $S_0$  emission seen in fluorescence spectra is related to the vibrational energy levels of the molecule and the energy of solvent reorientation. After the fluorophore has been excited to higher vibrational levels of the first excited singlet state ( $S_1$ ), excess vibrational energy is rapidly lost to surrounding solvent molecules as the fluorophore relaxes to the lowest vibrational energy level of the excited state. This process is called vibrational relaxation and occurs on the picoseconds timescale. Since the electronic configuration of the excited state is different from the ground state the solvent dipoles reorient to minimize interaction energy. This solvent relaxation is somewhat slower and occurs over tens of picoseconds. This lower energy of the excited state causes the emitted light to have a longer wavelength than the excitation light and this is called the Stokes shift [100]. There is some ambiguity in the Stokes shift definition. On one hand the Stokes shift can be defined as the difference in energy between the lowest vibrational levels of the  $S_1$  at the excitation and of the solvent relaxed  $S_1$  (the 0-0 transition). On the other hand for practical purposes it may be more interesting to know the shift between the most probable excitation and emission seen as the peak to peak distance. Both these definitions are used and while the first one only contains information on solvent relaxation energy the latter includes also some vibrational relaxation energy [101].

Internal conversion is the rapid non-radiative process where the excited states of the same multiplicity combine, *i.e.* singlets or triplets. This, together with vibrational relaxation populates the lowest vibrational state of the lowest excited electronic state. It is also possible to have internal conversion to the ground state resulting in a non-radiative deactivation. Intersystem crossing is the non-radiative process involving a transition between electronic states of different multiplicity, *i.e.* singlet to triplet or *vice*

*versa*. When changing multiplicity one of the unpaired electrons reverses their spins. Phosphorescence is the radiative relaxation involving a change in multiplicity, commonly from  $T_1$  to  $S_0$ . Processes including changes in multiplicity progresses on slower time scales than the other relaxation processes.

While all of the above processes are intramolecular, there are also interactions with other molecules that affect the excitation and emission of a molecule. Such processes will reduce the emission and in that respect they are referred to as quenching. Quenching can be a static phenomenon where molecules interact and thereby affect the ground state. A static quencher lowers the emission intensity, but does not affect the fluorescence lifetime (see below). Dynamic quenching occurs through interaction of the excited molecule with another molecule. Depending on the mechanism the dynamic quenching could be separated into three categories. Two fluorophores, mainly aromatic hydrocarbons, can form an excited dimer, an excimer [102, 103]. The excited molecule forms an excited dimer together with a ground state molecule. This excimer undergoes deactivation similar to single molecule, but since the energy gaps are different the emission wavelength is affected. Two of the dynamic processes involve energy transfer from one molecule to another [104, 105]. In both cases excitation energy is transferred from the excited donor to the acceptor molecule. The result is an excited acceptor and a ground state donor. The two processes have different mechanisms and work over different length scales. Dexter energy transfer [104] is a short-range phenomenon that depends on the donor and acceptor molecular orbitals having a spatial overlap. This is required since the energy is transferred through an exchange of electrons; moving the high energy electron to the acceptor molecule in exchange for a lower energy electron. The close range needed for this mechanism has rendered the term collision quenching. Förster resonance energy transfer [105], FRET, can transfer energy non-radiatively from the donor to the acceptor over larger distances (several nanometres) than Dexter energy transfer. The efficiency of FRET is governed by the distance between the donor and the acceptor, the spectral overlap of the donor emission and the acceptor absorption, and also the relative orientation of the dipole moments of the donor emission and the acceptor absorption. These dynamical processes, especially FRET, have given rise to numerous spectroscopic techniques used widely.

The emission efficiency of a fluorophore is described by the quantum yield,  $\Phi$ . It is the ratio between the amount of photons emitted by a molecule through fluorescence and the amount of photons absorbed by the same molecule as defined in equation 8:

$$\Phi = \frac{\text{Photons emitted}}{\text{Photons absorbed}} = \frac{k_F}{\sum_i k_i} \quad (8)$$

where  $k_F$  is the fluorescence rate constant and  $k_i$  are rate constants for all processes in the transition from the excited state to the ground state, including  $k_F$ . The partitioning between the relaxation processes, seen in Figure 5, might be affected by the solvent environment. A rigid environment is commonly fluorescence enhancing, *i.e.* a larger portion of the relaxation events will be emission of a photon. The average time in which a molecule occupies an excited state before it returns to the ground state is referred to as the fluorescence lifetime (equation 9).

$$\tau = \frac{1}{\sum_i k_i} \quad (9)$$

This lifetime is inversely proportional to the sum of rate constants of the processes involved in the transition from the excited state to the ground state as seen in equation 9 (*cf.* the second equality in equation 8)

### 4.2.3 Scattering of light

Two general principles regarding light scattering apply. The energy of the scattered photon might be the same as the energy of the incoming photon. Such scattering is called elastic scattering and different models will be discussed below. When the scattered light has a different energy than the incoming light the scattering is referred to as inelastic. At ambient temperature inelastic scattering generally imply emission of lower energy light. This section will describe scattering of light as defined above, but both elastic and inelastic scattering processes occur for high energy radiation as well (x-rays and  $\gamma$ -rays) [106, 107].

The theory for elastic light scattering by small particles in an ideal solution was derived by Lord Rayleigh [108] and is commonly referred to as Rayleigh theory. The particles should be much smaller than the wavelength ( $\lambda$ ) of the light being scattered for the Rayleigh theory to be valid. The upper limit of the particle radius of gyration for scattering of visible light is 20-40 nm. A more complex model is required for scattering solutions with non-spherical particles or with particles that are larger than required for the Rayleigh theory to be valid. This problem was solved regarding spheres by Mie [109]. The probability of a scattering event can be described by the scattering cross-section. The scattering cross-section is different from the geometric cross-section of the particle and depends on the wavelength of the light, and the shape and size of the particle. In correlation the extinction coefficient for light

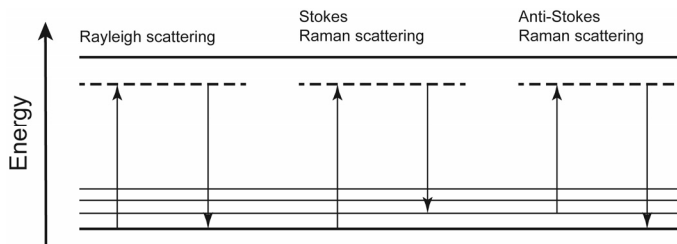


Figure 6 Jablonski diagram showing the energy levels of scattering. Electronic states are shown by thick lines and vibrational sub-states by thinner lines. The dashed line is the virtual energy level of the excited state. Radiative transitions are shown by solid vertical arrows.

absorbance (equation 11) can be expressed as absorption cross-section. For small particles the scattering cross-section follows the Rayleigh theory and depends on wavelength as  $\lambda^4$ . As the particles becomes larger, approximately the size of the wavelength, the wavelength dependence of the scattering cross-section is weaker than  $\lambda^4$ . In the Jöbst approximation [110], where the cases of the particle being either smaller or larger than the wavelength is considered, the cross-section wavelength dependence approaches  $\lambda^2$ . For non-spherical particles the theories above do not hold, but the Rayleigh-Gans method [111, 112] considering additional shapes for particles can be applied. As an example the scattering cross-section for long thin rods varies with wavelength as  $\lambda^3$ . It is inferred that the wavelength dependence of light scattering by particles is in the range of inverse fourth power for small particles to inverse square for larger or more asymmetrical particles. Numerical calculations for ellipsoids were done and the exponent was found to be decimal values in this range [113] which also was seen experimentally for bacteria.

The light causes the electron cloud of the particle to oscillate with the frequency of the incoming light. This oscillation results in a separation of charges called an induced dipole moment. In this process the photon is absorbed. For elastic scattering the energy is emitted as a photon of the same energy. This photon may leave the particle in any direction, although all directions may not be equally probable (larger particles Mie theory [109]). For inelastic scattering the emitted photon has a different energy than the incoming photon. The energy difference is characteristic for the material and corresponds to vibrational modes of the system. While there is strong particle size dependence in the elastic scattering cross-section, the inelastic scattering cross-section is small but independent of particle size and will be observed also for molecular solutions [114]. The inelastic scattering of visible light is called Raman scattering [115, 116] named after one of its discoverers. The energy levels and photon events in scattering is illustrated in a Jablonski diagram in Figure 6. If the final

vibrational state is more energetic than the initial state, then the emitted photon will have a longer wavelength than the incoming photon. This shift in wavelength is called a Stokes shift [100]. If the final vibrational state is less energetic than the initial state, then the emitted photon will be shifted to a shorter wavelength, an anti-Stokes shift. Anti-Stokes shift will only occur at elevated temperatures.

## 5 Analytical techniques

### 5.1 Spectroscopic techniques

#### 5.1.1 Absorption spectroscopy

Absorption spectroscopy is perhaps the most fundamental optic technique. A schematic image of a spectrophotometer for measuring absorption spectra is found in Figure 7.

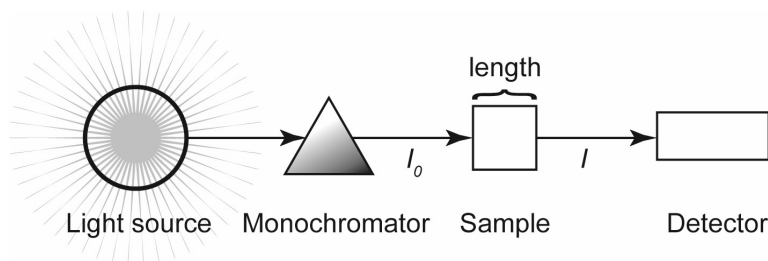


Figure 7 Schematic picture of a spectrophotometer and its components.

Absorption spectroscopy measures the ability of a sample to absorb light energy of a given wavelength. The intensity of light decreases as it passes through the sample and interacts with the molecules. The light intensity measured after the sample ( $I$ ) is related to the incident light ( $I_0$ ) by the wavelength dependent absorbance ( $A$ ) in equation 10.

$$I = I_0 \cdot 10^{-A(\lambda)} \quad (10)$$

The absorbance of a sample depends on the concentration of absorbing molecules ( $c$ ), the path length ( $l$ ) through the sample according to the Beer-Lambert law (equation 11).

$$A(\lambda) = \varepsilon(\lambda)cl \quad (11)$$

The extinction coefficient,  $\varepsilon$ , is a molecular property describing the light absorbing ability of the substance. The absorbance of a mixture is the sum of the separate absorbances of all the absorbing components. It can be said that the absorbance signals are additive. As seen above the light may also be scattered by particles in the

sample. The attenuation ( $\alpha$ ) describes the complete loss of light intensity during the sample passage due to absorption ( $A$ ) and scattering ( $S$ ) and could be used in place of  $A$  in equation 10 for a complex sample.

$$\alpha(\lambda) = A(\lambda) + S(\lambda) \quad (12)$$

For a scattering sample studied in a regular spectrophotometer the loss of light will be shown as absorbance. Here the effect of scattering particles on the transmitted intensity ( $I$ ) will be shown. In analogy with equation 10 the measured light intensity can be related to the incident light by a wavelength dependent expression.

$$I = I_0 \cdot 10^{-S(\lambda)} \quad (13)$$

Light scattering is commonly denoted in the natural logarithm while absorbance on the other hand uses the base 10 logarithm. The amplitude of light scattering, in analogy to equation 11, depends on the amount of particles in the sample (here described as a concentration,  $c$ ), the light path travelled ( $l$ ) and a wavelength dependent component (here denoted  $\tau(\lambda)$ ).

$$S(\lambda) = \frac{\tau(\lambda)cl}{\ln 10} \quad (14)$$

In scattering theory the particle concentration is often referred to as the number of particles per unit volume. The concentration effect on scattering in absorption spectroscopy is illustrated in Figure 8A.

In absorption spectroscopy in the regular UV-Vis range the scattering amplitude due to small particles (radius of gyration  $<40$  nm) following the Rayleigh theory will be strongly wavelength dependent. A simplified expression is given in equation 15.

$$S(\lambda) = p\lambda^{-4} \quad (15)$$

The parameter,  $p$ , is composed of several solvent and particle parameters as well as concentration and path length found in equation 14. This  $k$  can be treated as constant for any given sample. For larger particles not in the Rayleigh regime this equation can be generalized to equation 16 according to the discussion on light scattering above.

$$S(\lambda) = p\lambda^{-n} \quad (16)$$

The  $n$  describes particle properties and can have a value smaller than or equal to 4.

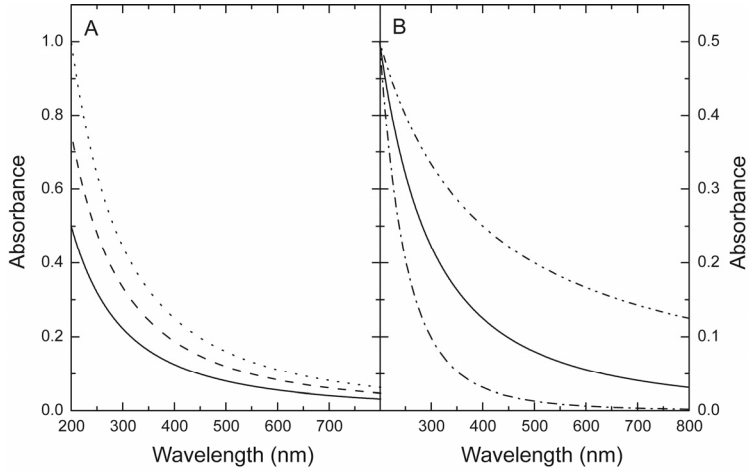


Figure 8 Scattering curves calculated from equations 14 and 16. A. Varying the concentration for a single particle size ( $n=2$ ). The concentrations (a.u.) in equation 16 are set to 1 (solid), 1.5 (dashed), and 2 (dotted) respectively. B. Varying the particle size at constant concentration using  $n=4$  (dash dotted),  $n=2$  (solid), and  $n=1$  (dash dot dotted).

The influence of  $n$  on the scattering signal in absorption spectra are shown in Figure 8B. Absorption spectra of samples that both absorb and scatter light consist of two components according to equation 12. If the light scattering component could be subtracted from the spectrum the absorbance part could be extracted. In this way techniques based on absorption spectroscopy could be used even for samples that contain light scattering particles. In order to extract the absorbance component of the signal the scattering part must be identified. The scattering is described by equation 16 but the two constants ( $p$  and  $n$ ) must be determined for the sample. The necessary information for determining these constants can be found in a recorded spectrum of the particles. Light scattering is seen as a characteristic curve, where the amplitude increases exponentially with decreasing wavelength. For a purely scattering sample this curve could be fitted to an exponential function as in equation 16. A convenient method to identify the scattering component is to use a logarithmic representation of the data. In a log-log graph the scattering signal will appear as a straight line [117, 118] corresponding to equation 17, which is a logarithmic version of equation 16.

$$\log S(\lambda) = \log p - n \log \lambda \quad (17)$$

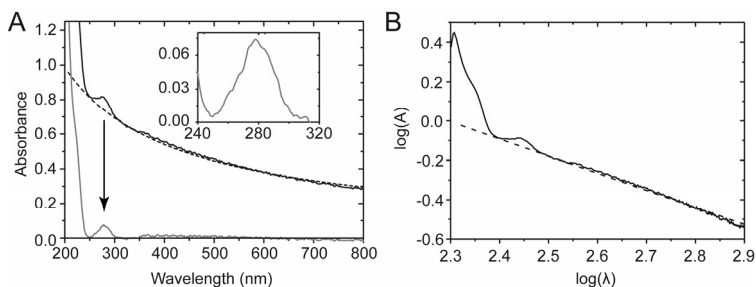


Figure 9 Example of the absorption correction procedure applied. A. The absorbance signal of the particle sample (solid) is composed of light scattering (dashed) and protein absorbance (gray). B. In a double logarithmic plot the scattering (dashed) can be fitted to a straight line and subtracted, revealing the protein absorbance (A inset). The slope of the line depends on the size and shape of the particles.

Data in this format can be fitted using linear regression where the slope and intercept of the line gives constants  $n$  and  $p$  respectively.

When the sample also contains an absorbing compound the log-log representation will deviate from the straight line at wavelengths where this compound is absorbing. If a sufficient wavelength range can be found outside the absorbance range, the scattering could be determined in that range using the same procedure of linear regression and then extrapolated into the rest of the spectrum range. An example of this procedure is shown in Figure 9. The case where the absorbing molecules and the scattering particles interact will be discussed further below in this chapter.

If the molecules in the sample absorb light of most wavelengths the procedure described above cannot be used to determine the light scattering component. However, there is nothing that prevents the scattering component to be subtracted once it is known. The only difficulty is to determine the shape of the scattering component. For a multitude of assays based on absorption spectroscopy the result is given by the absorbance at a single monitoring wavelength. For a given set of particles the  $n$  should be constant and the concentration is reflected by the  $p$  (equations 14 and 16). Two points on a scattering curve with a given  $n$  will always have a constant amplitude ratio. In paper X we developed a simple method to correct the absorbance at a single wavelength using the recorded attenuation where there should be no absorbance.

$$A_{corrected}(\lambda_{monitor}) = A_{observed}(\lambda_{monitor}) - kA_{observed}(\lambda_{no\ abs}) \quad (18)$$

In equation 18 the constant  $k$  is empirically determined for each type of scattering sample.

One of the basic requisites for the Beer-Lambert law (equation 11) is that the absorbing molecules (chromophores) should be evenly distributed in the sample volume. In a sample where the chromophores are confined in particles the recorded absorbance (when corrected for light scattering, see above) will be lower than the corresponding absorbance of the same amount of chromophores in solution. In other words, measurements on absorbing suspensions yield lower absorbance signals than measurements on the corresponding solutions. This phenomenon is called absorption flattening, and this name will be explained below. The effect is perhaps easiest to grasp using a projection of the suspension on a plane perpendicular to the light path (similar to the detector area). If the suspension is dilute it will be obvious that there are areas in this projection that contain no particles. Light passing through these areas will reach the detector irrespective the amount of chromophores in the particles. In contrast to solutions there will always be light transmitted through a dilute suspension. It shall also be stated that the average absorbance of a suspension and a solution are the same, but the instrument will instead average the transmitted intensities while calculating the absorbance. This effect is more pronounced when the absorbance of the particles is high. The reduction of the recorded absorbance will be highest closest to the peaks of the absorbance spectrum. Hence, the spectrum of a suspension will appear flatter than the corresponding spectrum of a solution giving rise to the name, absorption flattening.

Several models describing absorption flattening have been presented (see *e.g.* [119-121]). Recently Halling [122] made a simulation study exploring the different models. In his simulation work Halling identifies some key suspension parameters, all dimensionless. The parameters used to describe a suspension are the optical path length of the sample divided by the particle diameter ( $L$ ), the volume fraction of particles ( $\Phi$ ), and the absorbance of each particle ( $A_{part}$ ). The flattening coefficient ( $Q_A$ ) is used to relate the absorbances of suspensions and solutions (equation 19).

$$A_{suspension} = Q_A \cdot A_{solution} \quad (19)$$

Three models are identified and examined. In the first one presented by several studies [119, 123-126] the  $Q_A$  is found to depend only on  $A_{part}$ . In the second one [120],  $Q_A$  is found to depend on  $A_{part}$ ,  $\Phi$ , and  $L$ . The third model [121] finds  $Q_A$  to

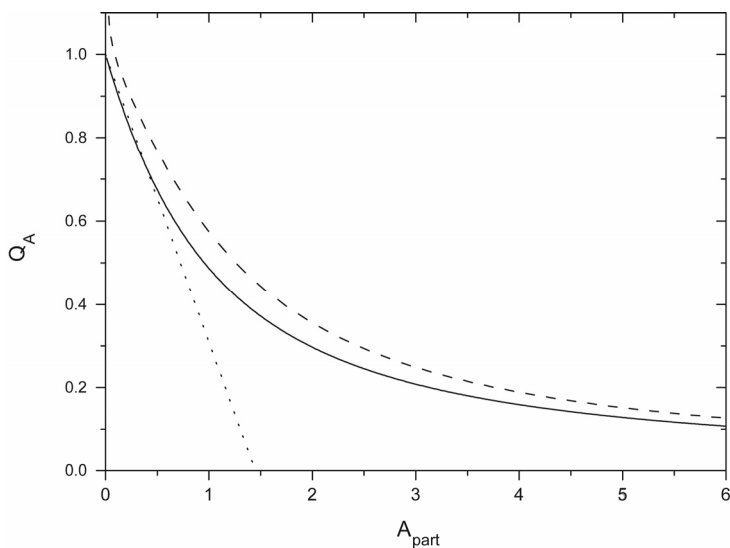


Figure 10 Predicted  $Q_A$  values from model equations [119-121]. The different models are represented by solid [119], dashed [120], and dotted [121] lines respectively. Adapted from Figure 2 of [122].

depend on  $A_{part}$ ,  $\Phi$ , and  $L$  as well as path length, wavelength and particle concentration. The  $Q_A$  dependences on  $A_{part}$  for the three models are illustrated in Figure 10. In Halling's study it is found that the first model agrees well with simulations for low  $\Phi$ . The second model is better for higher  $\Phi$ , but fails at low  $A_{part}$ . The third model yields similar values as model one in the low  $A_{part}$  range before it fails at higher values.

### 5.1.2 Fluorescence spectroscopy

Fluorescence spectroscopy is generally considered to be more sensitive than absorption spectroscopy. A schematic image of a fluorimeter used for fluorescence spectroscopy is shown in Figure 11. An emission spectrum is generated by illuminating the sample at a constant wavelength and recording the intensity as a function of the emitted wavelength. For an excitation spectrum the emission intensity at a constant wavelength is recorded while the excitation wavelength is varied. There are a wide range of assays based on fluorescence exploiting a number of observable properties such as emission intensity, wavelength shifts, or fluorescence lifetime (see equation 9) that can be correlated to the system property of interest. By monitoring emission over time the kinetics of a process can be followed.

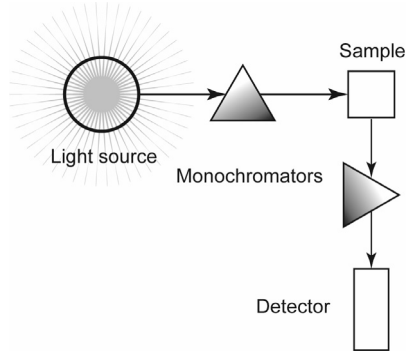


Figure 11 Schematic illustration of the components of a fluorimeter.

When the sample is excited by linearly polarized light an average oriented excited population is generated. If the excited fluorescent molecules, fluorophores, are not allowed to move until they emit their energy the emission will be polarized as well. This property is called fundamental anisotropy,  $r_0$  [127], and depends on the angle between the absorption and emission transition dipoles,  $\beta$ , as seen in equation 20.

$$r_0 = \frac{2}{5} \left( \frac{3 \cos^2 \beta - 1}{2} \right) \quad (20)$$

The intrinsic anisotropy is measured in the same way as the anisotropy,  $r$ , as described below. If the fluorophores are free to move they will rotate during the excited state lifetime and be less oriented when emitting. The anisotropy will then further depend on the relation between the lifetime,  $\tau$ , and the rotational time constant,  $\phi$ , according to equation 21. The anisotropy is calculated (equation 21) from the intensities recorded with the emission polarizer arranged vertically ( $I_{\parallel}$ ) and horizontally ( $I_{\perp}$ ) [128], when the sample is excited with vertically polarized light.

$$r = \frac{I_{\parallel} - I_{\perp}}{I_{\parallel} + 2I_{\perp}} = \frac{r_0}{1 + \tau/\phi} \quad (21)$$

As described above (section 4.2.2) energy can be transferred from an excited donor molecule to an acceptor molecule over a distance by FRET [105]. The efficiency of FRET depends (not exclusively) on the spectral overlap of the involved electronic states and the distance between the molecules. The strong (sixth order) distance dependence in FRET has come to be used to indicate molecular proximity and also to measure inter- and intramolecular distances, the so called spectroscopic ruler [129].

In an emission spectrum (similar for excitation) there may be signals that do not originate in fluorescence, but in different scattering events (see chapter 4.2.3). Elastic scattering by particles in the sample will be seen as an intense peak centred on the excitation wavelength. This phenomenon is sometimes called excitation bleed-through. Generally this intense radiation may be harmful for the detector and is avoided by starting the emission scan at longer wavelengths. Inelastic scattering (Raman) is seen as narrow peaks at characteristic distances from the excitation wavenumber, corresponding to a characteristic energy. As an example, the Raman peak of pure water is red shifted (*i.e.* to lower energy) by  $3380\text{ cm}^{-1}$  relative to the excitation light. When translated to wavelength the size of this red shift becomes wavelength dependent (*cf.* equation 3), *e.g.* it is 29 nm for excitation at 280 nm and 96 nm at 488 nm.

### 5.1.3 Linear dichroism

Linear dichroism (LD) is a spectroscopy technique using polarized light. The LD is defined as the difference in absorption between light linearly polarized parallel ( $A_{\parallel}$ ) and perpendicular ( $A_{\perp}$ ) to an orientation axis[130].

$$LD = A_{\parallel} - A_{\perp} \quad (22)$$

In a randomly oriented sample, absorption of linearly polarized light will be the same regardless of the polarizing direction and consequently the LD will be zero. The occurrence of a non-zero LD can be used to confirm induced orientation *e.g.* binding of a small chromophore to oriented DNA. The sign of the LD signal tells whether the absorbing transition moment dipole (see equation 7) is arranged mainly parallel (positive) or perpendicular (negative) to the orientation axis. Orientation can be introduced to an isotropic sample either by *e.g.* Couette flow [131, 132] or by application of an electric field [133, 134]. LD can also be studied in permanently aligned samples such as stretched polymer films [135] and the stacked bilayers of a lamellar liquid crystal [136]. In this work LD was used with flow orientation in paper V while the liquid crystal stacked bilayers were used in III, IV and V.

The reduced linear dichroism,  $LD^r$ , is the LD normalized with the isotropic absorption (equation 23). In a sample with uniaxial orientation where the transition moments are at an angle  $\alpha$  relative to a molecular reference axis the  $LD^r$  can be described as in equation 23 (right equality). The  $S$  is the orientation factor that describes the orientation of the molecular reference axis versus the macroscopic

orientation axis. The orientation factor is 1 for perfect orientation and 0 for isotropic samples.

$$LD^r = \frac{LD}{A_{iso}} = 3S \frac{(3 \cos^2 \alpha - 1)}{2} \quad (23)$$

Deformation of a spherical vesicle in shear flow forms an ellipsoid with the major axis at a small angle relative to the flow direction [137-139]. The defining axis for bilayer binding chromophores is the membrane normal. If this system is considered to be a biaxial system [140] the  $LD^r$  can be described by equation 24 [141].

$$LD^r = 3S \frac{(3 \cos^2 \alpha - 1)}{2} \cdot \frac{(3 \langle \cos^2 \beta \rangle - 1)}{2} = \frac{3}{4} S (1 - 3 \cos^2 \alpha) \quad (24)$$

The angle between the normal and the long axis of the deformed vesicle,  $\beta$ , can be considered perpendicular to the ellipsoid long axis. This is an idealised geometry that is useful in interpreting binding angles to the vesicles. Any deviations from an infinitely long vesicle with its major axis in the flow direction are condensed in the orientation factor  $S$ . The  $S$  is commonly determined by analysing an LD signal from a transition moment dipole with a known angle relative to the molecular axis such as the nucleobases in DNA [142] or a reference dye in vesicles [143]. For shear flow orientation it has recently been developed a method to calculate the  $S$  from molecular geometry and flow data [144].

For permanently aligned samples, such as a liquid crystal,  $A_{iso}$  cannot be directly measured. It can however, be obtained by correcting the absorbance  $A$  measured for the oriented sample for the lack of sample isotropy.

$$LD^r = \frac{LD}{A_{iso}} = \frac{LD}{A + (LD^{\omega=0}/3)} \quad (25)$$

In the resulting equation 25 for  $LD^r$  [145] the LD measured at an angle is extrapolated to a grazing angle,  $\omega$ , perpendicular to the bilayer normal.

## 5.2 Standard protein assays

A common but not trivial question in biochemistry is how much protein there is in a sample and how to best find that out. This is also a key property in several of the studies in this thesis. There are many methods available for the determination of protein concentration in a solution. Here some of the most common analytical

methods and the mechanism they are based on are presented. The choice of method can be based on five major criteria: the amount of protein available, the concentration of the sample, the presence of any interfering chemicals in the sample, the specificity of the assay, and the ease and reliability of the assay [146]. The different assays presented here are based either on the light absorbing properties of the proteins themselves or on staining of the proteins by an extrinsic dye.

### **5.2.1 *Intrinsic protein absorbance assays***

The aromatic amino acid residues, tryptophan and tyrosine, and the peptide bonds in proteins absorb UV light. Although proteins may have very different composition the protein absorption spectrum is characteristic with two maxima, at 280 nm (aromatic residues) [147], and at approximately 200 nm (peptide bonds) [148]. Two separate methods for protein concentration determination have been developed based on the knowledge of the protein absorption properties. The first method is based on the peptide bond absorbance and is commonly measured at 205 nm. There are a large number of peptide bonds in any protein, hence; this is a highly sensitive absorption range. The absorption properties of the peptide bond is very consistent and changes only slightly for peptides of different sizes [149]. The main drawback of determining protein concentration by the peptide bond absorbance is that many other chemicals used in protein solutions also absorb in this wavelength range. Such chemicals may contain double bonds between carbon and oxygen or between two carbons absorbing light in this wavelength range. To achieve reliable measurements at 205 nm the buffers must be chosen carefully and the protein solutions should be free of such chemicals that may have been used in protein purification.

The second method using the protein absorbance for determining the protein concentration is based on the aromatic amino acid absorbance. The trouble with absorption by buffer components is reduced by using that the aromatic amino acid residues in the proteins absorb light around 280 nm. Generally the absorption is measured on 280 nm and the concentration is calculated using equation 11. The extinction coefficient of each protein depends on the amino acid composition. Using a solution of known concentration the extinction coefficient could be experimentally determined for this protein. Otherwise it could be calculated from the amino acid composition data of the protein of interest [150, 151]. There are general values of the extinction coefficient for estimating total protein content in a crude mixture [151]. The method of protein concentration determination at 280 nm has a drawback in the interference by contaminating nucleic acids that may be present in many biological

samples. Nucleic acids have a strong absorbance at 260 nm that may disturb the protein measurements. There is however a technique to determine the protein/nucleic acid ratio and in that way correct for the nucleic acid contamination [152].

One general benefit of ultraviolet light absorption methods is that they can be performed directly on the sample without addition of any reagents. This entails that they are very rapid and also that they are non-consuming, *i.e.* that the sample can be used for other analyses after the concentration measurement. On the negative side is the protein extinction variability at 280 nm and the sensitivity to interfering compounds that causes a need for pure samples.

### 5.2.2 *Extrinsic absorbance assays*

Two of the most common analytical methods used in biochemistry are colorimetric assays for protein concentration [153, 154]. These assays are based on a colour shift of an extrinsic molecule in presence of proteins. Here some colorimetric assays will be described; starting with the most commonly used one. In 1922 the use of the Folin phenol reagent [155] was proposed for measurement of proteins [156]. This method was not widely used until the protocol established by Lowry *et al.* in 1951 [153], giving the assay its common name. Although very commonly used, the mechanism of the reaction is not well understood. However, in short it combines reaction of copper ions with the peptide bonds under alkaline conditions with oxidation of aromatic amino acid residues by reduction of the Folin reagent [157]. A copper complex that absorbs red light is formed causing the solution colour to become blue. The concentration of proteins is calculated from the concentration of the coloured complex that is measured by the absorption at 750 nm. A modified assay replacing the Folin phenol reagent by bicinchoninic acid (BCA) [158] was later introduced. This assay that measures the absorption of a complex of copper and BCA at 562 nm is easier to perform and is becoming increasingly popular.

The second type of colourimetric uses colour shifts in a dye to determine the protein concentration. The textile dye Coomassie brilliant blue G-250 (CB) (Figure 12) was found to have both pH and protein binding sensitive [159] spectroscopic properties. Both these properties were used in designing the Bradford assay [154] for protein concentration determination. In acidic solution CB is red but when binding to proteins it turns blue. The absorption is measured at 595 nm and the protein concentration is related to the absorption increase. The mechanism of CB binding to proteins and the change in colour is not fully understood (see [160] for a study on the

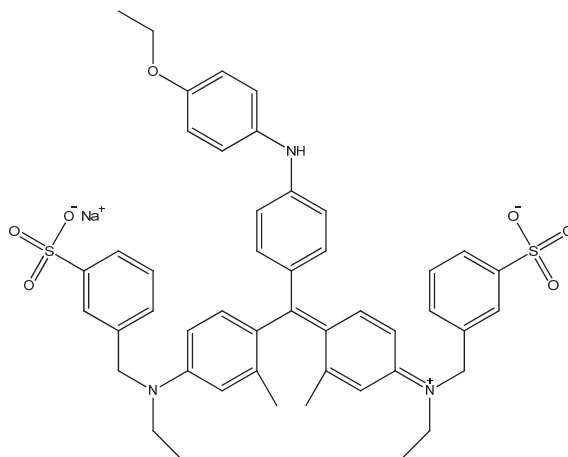


Figure 12 The protein binding dye Coomassie Brilliant Blue G-250 of the Bradford assay [154].

coloured forms of CB) but electrostatic binding mainly to the charged amino acid residues lysine and arginine [161, 162] is suggested. The details are debated and recently an assay based on an additional binding mode was presented [163]. Some properties of CB and the Bradford assay are discussed in papers XXI and XI outside this thesis. For all the colorimetric assays, the main drawback is the difference in colour yield for different proteins. The colour increase with protein concentration is only linear for a restricted interval; a drawback that all colorimetric methods suffer from.

### 5.2.3 Extrinsic fluorescence assays

In the last twenty years or so there has been a development of protein concentration determination assays based on fluorescence spectroscopy. In comparison, the fluorescence based methods have a higher sensitivity than the absorbance based ones commonly used. There has not yet been established any assay that is as commonly used as the older colourimetric assays. The different fluorescence assays use dyes of different kinds. Some of the commercially available assay are based on the protein binding properties of a merocyanine [164] (NanoOrange), styryl dyes [165] (Sypro red and orange), and ruthenium complexes [166, 167] (Sypro ruby), that all bind non-covalently or to surfactants covering the proteins. Another approach is to use dyes that react with free amines on the protein forming covalent attachments. Such dyes are for example CBQCA [168] and the naturally occurring dye epicoconone [169] that both changes spectroscopic

properties upon binding [170, 171]. The protein binding properties of epicocconone is further discussed in paper VII and below.

### 5.3 Electrophoresis

Electrophoresis is the motion of charged molecules or particles under the influence of an electric field. For electrophoresis in solution there are no barriers to molecular motion. A charged particle in an electric field will experience an accelerating electrical force,  $F_{el}$ . This accelerating force will depend on the charge of the particle,  $Q$ , and the strength of the electric field,  $E$  (equation 26). The particle will also experience a frictional force,  $F_{fr}$ , directed in the opposite direction to the electrical force. This frictional force depends on the translational frictional coefficient,  $f_t$ , and the particle velocity,  $v$  (equation 26).

$$\begin{cases} F_{el} = QE \\ F_{fr} = -f_t v \end{cases} \quad (26)$$

The particle will reach a steady state velocity where the accelerating and retarding forces are equal. The electrophoretic mobility,  $\mu$ , is defined as the velocity per unit field (equation 27).

$$\mu \equiv \frac{v}{E} = \frac{Q}{f_t} \quad (27)$$

In principle, all charged objects can be separated by electrophoresis. The most common analytes are duplex DNA [172] and proteins, either native in a pH gradient to determine pI (isoelectric focusing) [173] or denatured by the surfactant SDS (Sodium dodecyl sulphate) to determine size [174].

The DNA mobility in solution is independent of size above 400 base pairs [175]. In order to separate larger molecules, obstacles introduce size discriminating effects. This is achieved by performing the separation in hydrogels. In equation 27 this is represented by an increased friction from steric hindrance and collisions with the gel matrix. A large number of different hydrophilic gels have been employed for gel electrophoresis. The most commonly used are cross-linked polyacrylamide and agarose [172]. Because of their physical properties they are commonly used in different setups where the combinations of gel material and analytes have become standard. Polyacrylamide is used in thin gels, vertically between glass plates while agarose gels are thicker and submerged horizontally in buffer. In principle all

combinations are possible and many have been used *e.g.* horizontal slab polyacrylamide [176] and vertical SDS agarose [177].

For electrophoresis of amphiphilic biomolecules, both transmembrane proteins and proteins more loosely attached to membranes some special precautions have to be considered. First, the membrane proteins have to be extracted from the lipid membrane. This can be achieved by the use of surfactants [178]. Ionic surfactants are can be used to extract membrane proteins from their lipid environment. However, the use of ionic surfactants may result in denaturing of the analyzed proteins. Non-ionic detergents are milder and native membrane proteins may be solubilised for analysis. In both classes of surfactants a longer hydrophobic tail results in a milder solubilisation [179]. It seems that co-extraction of lipids may help the membrane proteins remain native. Second, the membrane proteins have to be kept solubilised during the experiment to prevent aggregation in the hydrophilic environment of the gel. There are protocols available both for native and denaturing electrophoresis experiments. In general, the optimal choice of surfactants for a given membrane protein is empirical [180]. There are guidelines for surfactant choice available, but optimization may be needed for all membrane proteins [179].

## 6 Applications of liquid crystals

In this chapter the most important results and conclusions in the amended papers I-V regarding my work with lyotropic lamellar crystals will be summarized and discussed. Some relevant unpublished results will also be presented.

### 6.1 Electrophoretic migration in a cubic phase

*The results in this section are from papers I and II.*

Electrophoretic separation of hydrophilic biomolecules based on *e.g.* size and isoelectric point is established as a technique with a wide usage (section 5.3). For amphiphilic biomolecules, especially transmembrane proteins, surfactant solubilisation approaches are used. There is no general protocol for solubilisation and the surfactants tend to affect the migrative velocity [181, 182]. With this in mind the diamond cubic phase (Figure 4) of monoolein and water was examined as a matrix for electrophoresis. This bicontinuous phase of curved bilayers contains a network of water-filled pores with a diameter of about 5 nm [19]. The monoolein bilayer is known to be able to incorporate transmembrane proteins for crystallization purposes. An especially attractive property of the monoolein-water system is that the cubic phase is stable in excess water [44, 183]. This allows for use of standard electrophoresis equipment with buffer reservoirs next to the electrodes. The monoolein bilayer is non-charged and ideally continuous over macroscopic distances. The diamond symmetry of the phase gives two networks of four-way water junctions with the pores meeting at an angle of  $109.5^\circ$  separated by one bilayer.

The electrophoresis separation matrix was prepared by first pouring melted monoolein in an electrophoresis tray. The tray was kept at  $8^\circ\text{C}$  to form a solid monoolein cake. This was then submerged in the electrophoresis buffer and swollen at  $37^\circ\text{C}$  for approximately 5 day until the monoolein was fully hydrated. The resulting phase was transparent, isotropic, and paste like and therefore assumed to be the diamond cubic phase. Probably due to inhomogeneities in the solid monoolein cake, the slab of cubic phase was uneven in thickness. An even surface was created by shearing off excess cubic paste with a spatula since an evenly thick gel is important for electrophoresis, forming a homogenous electric field. Due to impurities in the monoolein, probably oleic acid formed by hydrolysis, the electrophoresis experiments were done at low pH (4 and 5.6, respectively). At higher pH the cubic phase was affected and there was foaming at the ends of the monoolein slab. In a more recent

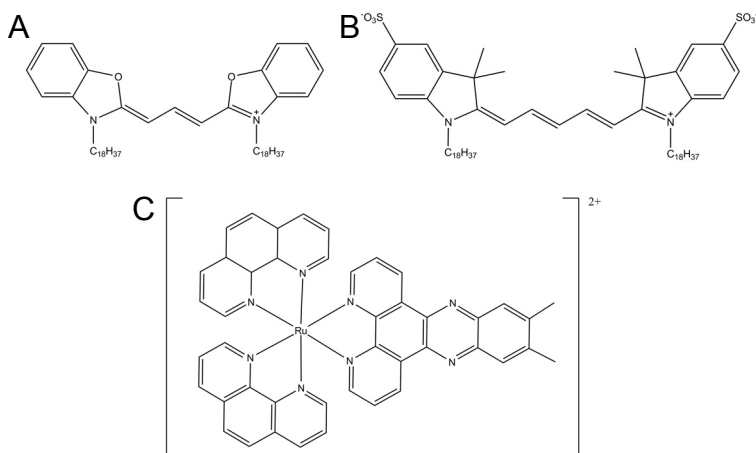


Figure 13 Membrane probes A. DiO-C18 B. DiI-C18-(5)-Ds C.  $[\text{Ru}(\text{phen})_2\text{Me}_2\text{dppz}]^{2+}$

review a wide range of amphiphiles that can form lyotropic liquid crystals in excess solvent are presented [184] perhaps opening a solution to this problem.

Short oligonucleotides and amphiphilic membrane probes (Figure 13) were used to study the electrophoretic properties of the cubic phase. The size of the oligonucleotides was similar to the water soluble part of a transmembrane protein. Both oligonucleotides and membrane probes were seen to migrate in the electric field. The velocity was constant with time and thereby the migrated distance, supporting the hypothesis of a homogenous cubic phase over mm distances. We found that the velocity was independent of analyte concentration both for migration in the water channels and in the bilayer membrane. This indicates that the origin of the retarding friction (equation 26) was interactions either between the oligonucleotide and the curved bilayer or between the membrane probe and the monoolein and not by *e.g.* interactions between oligonucleotides.

The velocity of both oligonucleotides and membrane probes were found to increase linearly with increasing field strength, *i.e.* the electrophoretic mobility (equation 27) is constant. The only exception is the fairly long and flexible 25-mer single stranded oligonucleotide, where the mobility increases with the field strength. This is likely due to perturbation of the oligonucleotide configuration by adaption to the shape of the water channel structure. The membrane probes most likely are inserted in the monoolein bilayer both during diffusion and during electrophoretic migration.

Table 2 Electrophoretic mobility in monoolein-water diamond cubic phase.

Probe	12-mer single <sup>1</sup>	12-mer double <sup>1</sup>	25-mer hairpin <sup>1</sup>	25-mer double <sup>1</sup>	DiI <sup>2</sup>	DiO <sup>2</sup>	[Ru(phen) <sub>2</sub> - Me <sub>2</sub> dppz] <sup>2+</sup> 2
Mobility (10 <sup>-6</sup> cm <sup>2</sup> V <sup>-1</sup> s <sup>-1</sup> )	6.1	2.4	3.2	0.83	2.5	1.8	3.9

<sup>1</sup> Data from paper I. <sup>2</sup> Data from paper II.

Both hydrophilic and amphiphilic analytes move as distinct zones in the cubic phase. The zone length (in the direction of the field) for oligonucleotides was found to increase linearly with time during electrophoresis. By changing the electric field strength it was concluded that the zone lengthening rather depends on the length migrated. This confirms the hypothesis that the zone lengthening is caused by a dispersion of the molecules induced by collisions with the monoolein bilayer network. The zone width (perpendicular to the field) increases by diffusion independent of the electrophoretic migration. The diffusion was systematically studied for a range of membrane probes. The size of the hydrophilic part of the membrane probes was more important for the friction than the size of the hydrophobic part. The slow migration of the membrane probes supports the hypothesis of them being inserted in the bilayer during electrophoresis.

In order to achieve electrophoretic separation the mobility of different samples must be different. The membrane bound probes have mobility values in the same range as the oligonucleotides examined (Table 2). For the water soluble oligonucleotides the mobility depends both on molecular weight and conformation. A flexible single stranded oligonucleotide migrates faster than the rigid double stranded.

## 6.2 Orientation of short oligonucleotides

*The results in this section are based on paper III (the sodium octanoate-decanol-water system) and some unpublished observations (the AOT-water system) [185].*

DNA interactions with cationic surfactants and cationic bilayers have been studied mainly as non-viral carriers of DNA for gene therapy purposes [186-188]. The DNA and surfactants can form ordered complexes upon mixing. There are examples of lamellar [186] and inverted hexagonal [188] symmetry of these complexes. Here the DNA is a central part of the lyotropic liquid crystal formation.

Without the DNA the lipids are forming liposomes. When binding to cationic bilayers the DNA molecules are confined to move in two dimensions only [189]. The nucleobases may become embedded in the apolar region of the membrane [190], causing reduction of the nucleic acid base-pairing capability. Less is known about the interactions between nucleic acids and membranes with net negative charge, such as the cell membrane. In one study DNA does not adsorb to negatively charged surfaces, unless the DNA net charge is reduced by cationic surfactants [191]. Even binding to a zwitterionic bilayer without the aid of cationic lipids or divalent cations is very weak [192]. In this thesis the behaviour of oligonucleotides together with bound dye molecules is discussed in section 6.3.

The lyotropic liquid crystalline phases used to study the oligonucleotide orientation were both lamellar. The major part of the results was obtained using the lamellar phase of the ternary system of sodium octanoate, decanol and water [193]. The phase diagram [194] shows a large region where this system forms a lamellar structure. Depending on the composition, the bilayer charge and the water domain thickness are different. In this study the bilayer composition and charge was kept constant at a 24/76 ratio between octanoate and decanol. The thickness of the water domain,  $d_w$ , was varied between 5 and 7 nm using equation 28 [194], where  $W_A$  is the weight fraction amphiphilic matter and the constant  $k = 2.32$  nm was determined from experimental data [195].

$$d_w = \frac{k}{W_A} \quad (28)$$

A larger range can be achieved according to the phase diagram but was not used. For the aerosol OT (AOT) and water system [196] the phase diagram is dominated by the lamellar phase and a large range of  $d_w$  could be prepared. AOT bilayer surface charge is  $-1$  for each molecule or  $-1/2$  per lipid tail. Both systems were previously used to orient dyes for linear dichroism [136].

The lamellar bilayer formation was confirmed with membrane probe dyes both by themselves (section 6.3.1) and in presence of the oligonucleotides. The liquid crystals had a macroscopic orientation with the bilayer normal perpendicular to the supporting quartz surfaces used for the spectroscopic studies. The oligonucleotides were found to be restricted to move in the plane of the water domain, perpendicular to the bilayer normal. No macroscopic order within this plane was found as the samples appeared isotropic when studied at a grazing angle of  $90^\circ$ , *i.e.* parallel to the bilayer normal. Single stranded samples do not become oriented by insertion in the

lamellar phase. The double stranded oligonucleotide remains a duplex in the liquid crystalline environment. This was concluded since a denatured helix would not exhibit any LD signal, just as the single stranded sample. The secondary structure of the double helix was determined, by the shape of the LD<sup>r</sup> spectrum, to be B-form [142], and could then be modelled as a rod with a diameter of 2 nm and a length of 8.5 nm. The length was longer than the water domain thickness making end-over tumbling unlikely. With increasing water content and thereby increasing distance between the parallel bilayers the degree of orientation decreased as seen in the LD<sup>r</sup> signal. This was explained mainly by that the oligonucleotide freedom to move in the out-of-plane dimension increased as the water domain thickness increased. The overall orientation of the bilayers simultaneously decreased, but to a lower degree due to higher bilayer flexibility.

The induced orientation makes the oligonucleotides suitable for linear dichroism (section 5.1.3) studies. This provides a possibility to study the geometry of DNA-dye interactions in a lipid rich environment and also provides a possibility to study interactions with designed DNA sequences in addition to a parallel study in the same lab [197, 198]. Common flow orientation in a Couette cell is restricted to longer DNA fragments [199] (~1000 base pairs) than the current practical limit of solid state DNA synthesis (~150 base pairs).

It is likely that the confining forces include long range electrostatic repulsion between the DNA and the anionic membrane as a significant part together with the steric confinement. Paper III does not address this question since the membrane surface charge density was kept constant. Further, the electrostatic effects are expected to be strongly shielded since the sodium ions of the octanoate, in addition to the sodium ions from the buffer, give rise to an average cation concentration of about 0.7 - 0.9 M in the water layers. The Debye screening length at such high monovalent salt concentration is small (0.3 nm) compared to the water layer thickness (5-7 nm) and the DNA diameter assumed (2 nm). Despite the fact that both the bilayer and the DNA are subject to strong counter-ion cloud screening, long-range electrostatic repulsion can be expected to have a significant ordering effect; however, systematic studies are difficult since with increased DNA lengths the steric confinement will dominate.

## 6.3 Dye – bilayer interaction

*The results in this section are based on papers II, III, IV, and V as well as some unpublished observations [200].*

### 6.3.1 Position and orientation of dyes

Orientation of dyes interacting with bilayers has been used for different purposes in this thesis work. In paper III the behaviour of DNA-dye interactions in a bilayer rich environment was studied. In paper IV the internal orientation of two transition moment dipoles in a membrane anchored dye was determined and in paper V the behaviour of three voltage sensitive dyes [201] was examined.

Small guest molecules such as dyes can interact with a bilayer in three distinct positions shown in Figure 14. The different positions are: A. Bound to the surface enhanced by electrostatic interactions, B. Inserted in the membrane parallel to the hydrophobic chains, and C. Solubilised in the bilayer centre. LD studies can help distinguish between directions parallel and perpendicular to the bilayer normal, *i.e.* between the A/C and the B positions. To distinguish between A and C additional information about the molecular hydrophilicity and hydrophobicity as well as spectral properties (section 6.3.2) in solvents resembling the different parts of the bilayer [202] is needed. In general the molecules interacting in the A position are charged (ehtidium bromide, rhodamine 6G) or polar (acridine orange, thioflavin T) without a strong amphiphilic character. The molecules found to insert in the bilayer according to B are amphiphilic with clear separation between the charged/polar and the apolar parts of the molecules (retinoic acid, orange II). Apolar molecules ( $\beta$ -carotene [136]) can be solubilised in the bilayer centre in the C position.

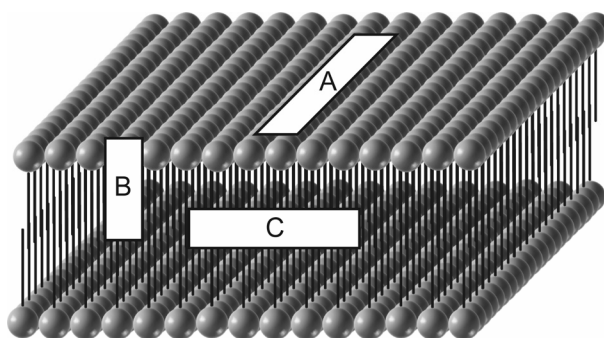


Figure 14 Schematic membrane probe orientations. A. Surface bound B. Inserted in the bilayer C. Bilayer centred.

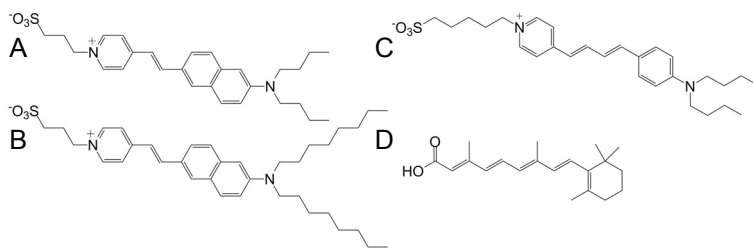


Figure 15 Membrane probes A. di4-ANEPPS B. di8-ANEPPS C. RH-421 D. Retinoic acid

Calculating the binding angle  $\alpha$  (equations 23 and 24) requires the orientation factor  $S$  to be determined by a reference signal with a known binding angle to the bilayer normal. For liposomes (equation 24) retinoic acid is the benchmark molecule for orientation in this lab. Retinoic acid has been assigned  $\alpha=0^\circ$  [143] and is used as a common reference. In paper V this was used to determine the insertion angle of three voltage sensitive dye molecules (Figure 15) in 4:1 DOPC-DOPG liposomes. We hypothesised that a strong alignment with the membrane normal should make the voltage sensitive dyes better suited to sense variations in the membrane potential. Using retinoic acid as the standard, the binding angles were determined for di4-ANEPPS, di8-ANEPPS, and RH-421 (Table 3). The results show, perhaps somewhat counterintuitive, that the shorter di4-ANEPPS is more aligned than the longer di8-ANEPPS. The lipid chains are more oriented parallel to the bilayer normal close to the bilayer surfaces and less oriented in the bilayer centre [203]. This bilayer property may be the cause of the higher orientation for the shorter molecule. In lamellar liquid crystals of sodium octanoate, decanol and water the three voltage sensitive dyes all are aligned stronger than the proposed reference retinoic acid. Therefore, no binding angles were calculated for this system. It shall be noted that the alignment was different between the two systems. In liposomes the orientation order is retinoic acid > di4-ANEPPS > di8-ANEPPS > RH-421 and in the lamellar liquid crystal it is di4-ANEPPS > di8-ANEPPS > RH-421 > retinoic acid. The surface charge is negative in both cases but lower for liposomes and the head groups are larger in the liposomes

Table 3 Apparent binding angles of the transition dipole moments of the probes in liposomes

Probe	di4-ANEPPS	di8-ANEPPS	RH-421
$\alpha_{\text{apparent}}^1$	$14^\circ \pm 4^\circ$	$18^\circ \pm 4^\circ$	$21^\circ \pm 4^\circ$

Using retinoic acid as a reference. <sup>1</sup> Data from paper V

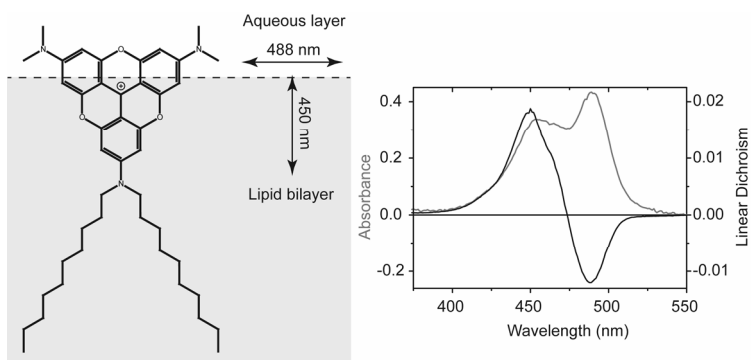


Figure 16 Left: Schematic position of ATOTA in a lipid bilayer with the orientation of the major transition dipole moments. Right: Linear dichroism and absorption measured on the oriented ATOTA in the lipid bilayer. Data are from paper IV.

compared to the lamellar liquid crystal bilayers. The bilayer thickness is approximately 2.5 nm for the liquid crystal system and between 4 and 5 nm for the DOPC-DOPG liposomes. The oriented dyes may be dimers since two different dimer models for the voltage sensitive dyes were suggested based on spectral data (section 6.3.2).

In paper IV the liquid crystal bilayer system was used to determine the relative orientation of two transition moment dipoles in the same dye, an ATOTA<sup>+</sup> derivative (2-didecylamino-6,10-bis(dimethylamino)-4,8,12-trioxatriangulenium). In dyes with high symmetry such as triphenylmethanes (*e.g.* Coomassie blue, crystal violet, and rhodamine 6G) the S<sub>1</sub>-state (section 4.2.1) may be degenerate [204]. If the charged dye and its counterion come into close proximity, the electric field of the anion will split the degenerate S<sub>1</sub>-state resulting in two absorption peaks. Three distinct interaction states of the ATOTA<sup>+</sup> dye and its PF<sub>6</sub><sup>-</sup> counterion were found in solvents of different polarity [205]. In polar solvents the dye was well separated from its anion and displayed a single absorption band from the degenerate transition. In apolar but polarisable solvents an ion pair was formed displaying two clear absorption peaks caused by symmetry breaking. In apolar and non-polarisable solvents, a dimer of ion pairs was formed. In our experiments the ATOTA<sup>+</sup> ion inserted in the bilayer (Figure 16) and this caused the absorption to split in two peaks. The two absorption peaks gave rise to one negative and one positive LD-peak (Figure 16). The red-shifted peak was mainly oriented perpendicular and the blue-shifted peak parallel to the bilayer normal. By introducing a molecular coordinate system where the red-shifted  $\alpha$  (equation 25) was 90° the orientation factor was determined. By using this orientation factor the angle for the blue-shifted  $\alpha$  was determined to be 15°. This was close enough to the predicted value of 0° to state that

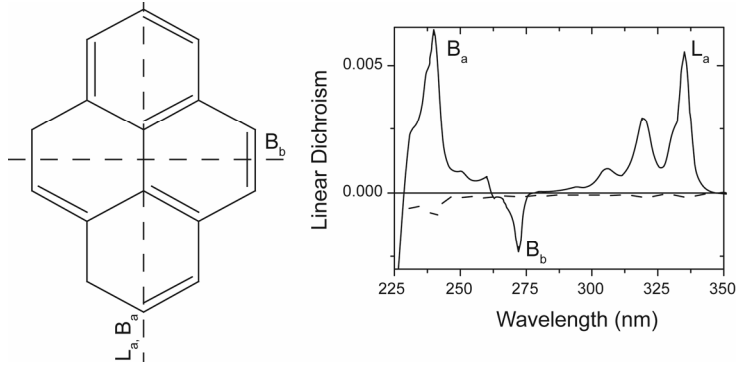


Figure 17 Left: Pyrene structure with transition moment dipole orientations. Right: Linear dichroism spectra recorded at grazing angles  $60^\circ$  (solid) and  $90^\circ$  (dashed) respectively, with the corresponding transition moment dipoles indicated. Data are from paper III.

the two transition dipole moments were orthogonal within experimental error. This provided experimental support to the quantum mechanical calculations of the peak splitting in paper IV.

In paper III the membrane probe pyrene [206] was used in the lamellar liquid crystal formed by sodium octanoate, decanol and water. The pyrene molecule inserted itself into the lipid bilayer with its long axis oriented parallel to the bilayer normal and the short in-plane axis perpendicular to the normal [206, 207]. The pyrene absorption contains three major bands, either with the transition moment dipoles oriented along the molecular long axis (the  $L_a$  (335 nm) and  $B_a$  (240 nm) peaks) or oriented along the short in-plane axis (the  $B_b$  (272 nm) peak) [208, 209] as shown in Figure 17. The sample appeared isotropic when observed at a  $90^\circ$  grazing angle. When the same sample was observed at a  $60^\circ$  grazing angle positive LD was observed at the wavelengths corresponding to the long axis transition moment dipoles ( $L_a$  and  $B_a$ ) while the short axis transition ( $B_b$ ) exhibited a negative LD-peak (Figure 17). This alternating pattern of LD signs corresponded to a pyrene orientation with the long axis parallel with the hydrophobic chains of the lipids in the bilayer. These absorption bands of pyrene have nearly no overlap of absorptions due to different transitions, so called pure polarization. In such case the order parameters,  $S$ , for the molecular axes can be directly obtained from the  $LD^r$  (equation 29):

$$\begin{cases} S_{xx} = 1 - S_{yy} - S_{zz} \\ S_{yy} = LD_{272nm} / (3 \cdot A_{272nm}) \\ S_{zz} = LD_{335nm} / (3 \cdot A_{335nm}) = LD_{240nm} / (3 \cdot A_{240nm}) \end{cases} \quad (29)$$

The ratio between the LD<sup>r</sup> peak values for the two orthogonal transitions L<sub>a</sub> and B<sub>b</sub> is equal to the ratio of the orientation factors  $S_{yy}/S_{zz}$  [210]. The calculated value  $-0.38$  is close to the value expected for a rod-like orientation ( $S_{yy}/S_{zz} = -0.5$ ) as opposed to, for example, the expected value for a disc-like orientation ( $S_{yy}/S_{zz} = +1$ ) [210]. This value is also very similar to what has been reported for pyrene bound to flow-oriented bicelles [53]. In the lamellar membrane system pyrene adopts a more rod-like orientation than what is observed in a uniaxial matrix of stretched poly(ethylene) where  $S_{yy}/S_{zz}$  is near zero [145].

Pyrene was found to be an excellent membrane probe and the fact that it behaves here nearly as a rod indicates that it experiences the tight proximity of the lipid alkyl chains near the polar head groups where they are well ordered. This shallow molecular position near the bilayer surface has been seen in both experiments and molecular dynamics simulations [206, 207, 211]. This positioning of the highly aromatic pyrene molecule has been explained either by the pyrene molecule having a partial charge similar to what is known for benzene [206, 207] or that the large rigid pyrene molecule for entropic reasons avoids the highly disordered bilayer centre in favour of the more ordered region near the head groups [211].

In paper III a series of well known DNA intercalators (ethidium bromide, YO-PRO-1, YOYO-1) were investigated together with 25-mer double stranded oligonucleotides (section 6.1) in the lamellar liquid crystal of sodium octanoate, decanol and water. In bulk solution all these molecules bind DNA, but in the bilayer system none of these DNA ligands were found to bind to the oligonucleotides. Since these DNA intercalators all are positively charged they may also interact with the negatively charged bilayer surface. Without DNA present, all three molecules showed negative peaks consistent with an alignment parallel to the lipid bilayers, position A in Figure 14. With DNA present no changes in the LD spectra could be detected. By considering the relative concentrations of binding sites on the DNA and on the membrane a possible thermodynamic explanation for this behaviour is provided. The concentration is  $15.6 \mu\text{M}$  of oligonucleotide duplexes in the water domain whereas the apparent concentration of head groups of the lipid bilayer surfaces can be considered to be  $1.8 \text{ M}$  for decanol and  $0.6 \text{ M}$  for octanoate, respectively.

Also in paper III, different dyes (Cy3, Cy5, FAM, and ROX) covalently attached *via* a flexible tether to the end of double stranded oligonucleotide helices were studied in the lamellar liquid crystal. It is known that Cy3 and Cy5 are prone to stacking to the end of the oligonucleotides like an additional base pair in aqueous solution, while FAM and ROX are freer to rotate. This behaviour is reported for the cyanine dyes

both in their sulfonate-free [212-214] and sulfonated [215] forms. The orientational behaviour of these dyes is important when used in FRET applications [216]. The oligonucleotides with the covalently attached dyes were incorporated in the water interstitia of the lamellar liquid crystal and oriented as described in section 6.1. We found by LD that oligonucleotide-bound Cy5 associates with the bilayer surface in this environment. The same behaviour was also seen for free Cy3 and Cy5, *i.e.* position A in Figure 14. In contrast, oligonucleotide-bound Cy3 was found to have dual LD peaks in opposite direction. The larger positive peak shows that Cy3 is mainly end-stacked, but a smaller, red-shifted negative peak shows that there is a subpopulation of Cy3 molecules that de-stack and associate with the bilayer surface. Oligonucleotide-bound FAM and ROX were not oriented by the lamellar liquid crystal, neither end-stacked nor surface bound.

### 6.3.2 Spectral effects of solvents and bilayer interaction

The local environment might be responsible for the function of voltage sensitive dyes through solvatochromism. It is debated whether the voltage sensitive dyes changes colour due to electrochromism (electron configuration changes with bilayer potential) or solvatochromism (dye position changes with bilayer potential) or a combination of the two [217]. Solvatochromism is the solvent polarity dependence of the colour of a dye. Here I will consider the two ANEPPS derivatives used in paper V (Figure 15) because they contain the same chromophore. The spectral differences seen between these molecules should originate from the local molecular environment. Absorption and emission spectra were recorded for the dyes in different solvents (water and alcohols) of decreasing polarity and in the two bilayer model systems (lamellar liquid crystal and liposomes). In addition to experiments quantum mechanics calculations were performed for dye monomers in all solvents and also for a parallel and an anti-parallel dye dimer in the most polar and apolar solvents determining absorption peaks. In water experimental absorption data and calculations combined suggest formation of aggregates with the chromophores aligned parallel to each other. The emission difference and also experiments in glycerol-water mixtures indicate stronger di8-ANEPPS aggregates. This corresponds well to the slow bilayer incorporation seen for this dye. In alcohol solvents both ANEPPS dyes appear as monomer except for decanol where the combination of absorption and calculations suggest anti-parallel dimers. For the monomer dyes the absorption peak red-shifts and the emission peak blue-shifts decreasing the Stokes shift with decreasing polarity. In the bilayers two different dimer configurations are suggested. For the liquid crystal membrane the voltage sensitive dyes are all longer than the hydrophobic tails of one monolayer. The combination of experimental data

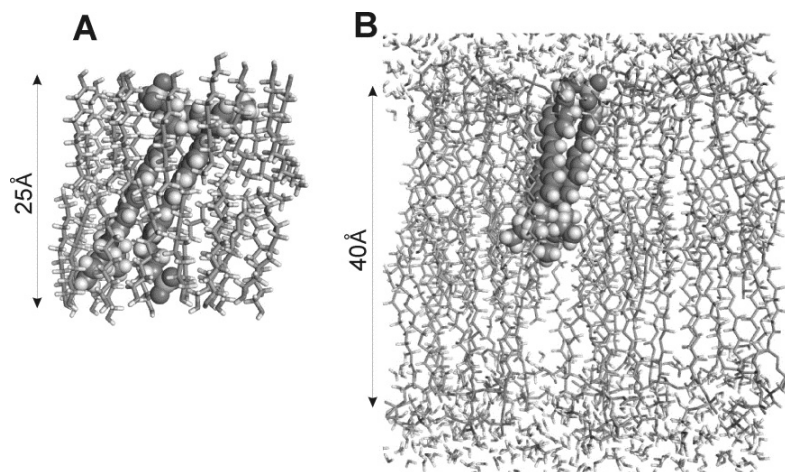


Figure 18 Length and estimated orientation of the antiparallel and parallel dimers of di-4-ANEPPS in a decanol bilayer (A) and in a lipid bilayer (B). Schematic representations were built using PYMOL. Reprinted with permission from paper V. Copyright 2012 American Chemical Society.

and calculations suggest an anti-parallel dimer configuration in the thinner lamellar liquid crystal bilayer spanning the whole bilayer (Figure 18). In the thicker liposome bilayer this configuration would not be preferred. Here the data suggest a parallel dimer arrangement anchored in one of the bilayer surfaces (Figure 18).

In paper I the emission of oligonucleotide bound Cy5 in the monoolein-water cubic phase was seen to decrease with time in acidic buffer (pH 4). We concluded that it was in fact the dye that lost its fluorescence and not loss of dye from the oligonucleotide zone in the monoolein-water matrix. The emission was measured over time both in the cubic phase and in pure buffer at different pH values. The half-life of the dye was seen to be clearly pH dependent in buffer. We found that the laboratory light had no strong bleaching effect over the course of the experiment. The fluorescence loss was reduced by about one order of magnitude by incorporation in the monoolein-water cubic phase at pH 4 as compared to solution. When an electric field was turned on (section 6.1) the protecting effect of the bilayer rich environment was reduced, but not all the way back to the solution value. Emission spectra in different solvents and the cubic phase were recorded. A shift was observed between buffer and the monoolein cubic phase. This shift was smaller than *e.g.* the shift between buffer and ethanol and from this we concluded that Cy5 associated with the bilayer as in position A in Figure 14. An insertion as in position B would have caused a larger shift. In addition to be sensitive to pH Cy5 has also been found to be sensitive to ozone in a microarray setup[218].

## 7 Spectroscopic studies of immobilized enzyme

In this chapter the central parts of the work on immobilization of enzymes in mesoporous silica in the amended papers VI-VIII will be summarized and discussed.

### 7.1 Spectroscopic effects of particle suspensions

*The results in this section are based on papers VI and VII as well as some unpublished observations [200, 219].*

The immobilization of enzymes in mesoporous particles changes the spectroscopic properties of the sample compared to having an enzyme solution. With particles present the suspension will appear milky white when observed by eye. In absorption spectroscopy it will be seen as an elevated signal over all wavelengths. The amplitude of this signal will increase with decreasing wavelength as seen in Figure 8. In section 5.1.1 and Figure 9 methods to remove this scattering signal are explained. In paper VII, by using the linear regression method (equation 17, Figure 9), the ultraviolet absorption of BSA and lipase could be separated from the recorded data. The lower the protein to particle ratio the harder the detection becomes. It was possible to identify the absorption peak at the protein-to-particle ratios used in paper VII (60 and 100  $\mu\text{g}/\text{mg}$ ). For a given ratio the absorbance and scattering will both be decreasing with decreasing concentration. A linear relationship between the corrected absorbance and particle concentration was found up to the highest particle concentration tested, approximately 2 mg/ml. At very high particle concentrations where the recorded absorbance is above 1 the corrected absorbance is lower than expected.

In addition to the effect of light scattering, immobilization may also cause absorption flattening (5.1.1). This effect is caused by the uneven distribution of the absorbing molecules in particle suspensions. Experiments were made by immobilizing BSA covalently stained with pyrene into mesoporous silica particles [219]. The pyrene was covalently attached to the protein by the same linker chemistry that was used for SNARF-1 in paper VI. Pyrene was chosen because the distinct narrow absorption peaks aid the spectra interpretation. BSA has been used as a standard protein in several of the studies in this thesis. The addition of the dye increases the extinction coefficient (equation 11) and thereby enhances the effect of absorption flattening. The stained BSA was immobilized into mesoporous silica particles (diameter 1  $\mu\text{m}$ , pore diameter 9 nm) by physical adsorption. Given the pore

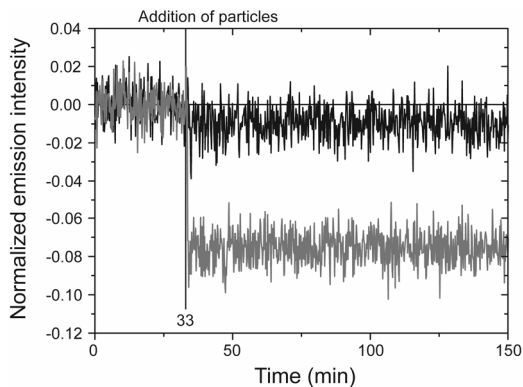


Figure 19 Normalized emission of di4-ANEPPS in ethanol. At 33 minutes mesoporous silica particles (diameter 1  $\mu\text{m}$ , pore diameter 9 nm) were added to the samples to a final concentration of 70  $\mu\text{g/ml}$  (black) or 550  $\mu\text{g/ml}$  (grey).

loading and the pyrene extinction coefficient the  $A_{part}$  (Figure 10) is approximately 0.07. As seen in Figure 10 this corresponds to the upper left corner and according to the first model where  $Q_A$  depends only on  $A_{part}$  [119, 123-126] the  $Q_A$  is determined to be approximately 0.94. Using equation 19 a recorded absorbance of 0.08, after correction for light scattering (equation 17), corresponds to an absorbance of 0.085 for the same amount of enzyme in solution. In paper VII the  $A_{part}$  was low and  $Q_A$  was considered to be close to 1 and not treated separately.

When using fluorescence spectroscopy the presence of particles will affect the recorded signal in several ways. Firstly, some of the excitation light will be scattered in the direction of the detector and seen if the emission is recorded at wavelengths close to the excitation wavelength (excitation bleed-through, section 5.1.2). If the Stokes shift is large enough this does not affect the data. Secondly, the amount of fluorophores getting excited in the detection volume will be lower. This is caused by the scattering lowering the intensity of the excitation beam. Less excited fluorophores will result in lower emission from the sample. Thirdly, the emitted light will also be scattered by the particles. This effect will be lower than the scattering of the excitation light due to the wavelength dependence of the scattering cross-section. The magnitude of the latter two effects will depend on the experimental setup. To my knowledge no theoretical studies on these scattering effects have been published to date. The effect of mesoporous silica particles was examined in an unpublished experiment [200] using a solution of di4-ANEPPS (Figure 15) in ethanol. The dye is here a unimer as determined in paper V. Mesoporous silica particles dissolved in

ethanol were added to the dye solution. The emission intensity is seen to decrease when the particles are added (Figure 19). Under these conditions the dye does not enter the pores to any large extent as seen on the particles when they were removed by centrifugation and by supernatant absorption. The effect here of inert silica particles is lowered emission intensity. Within these particle concentrations the effect seems to be increasing with increasing particle concentration.

The emission intensity was seen to be affected by the presence of particle, but what about the emission spectral shape? In the same experiments with di4-ANEPPS in ethanol solution with added mesoporous silica particles the shapes of the emission spectra were examined. By normalizing the spectra the emission spectral shape was found to be virtually unaffected by the presence of the particles. The only differences were seen at short wavelengths and could be attributed to excitation bleed-through. The main peak was unaffected by the particles. Based on the effects of scattering in fluorescence spectroscopy some general guidelines can be established. Assays based on spectral effect should be easier to adapt to particle samples than assays based on changes in emission intensity. However, caution should be applied towards spectral changes caused by molecular interactions and solvent composition rather than the examined property, *e.g.* the effect of a butanol-water mixture in paper VII described in section 7.4.

## 7.2 Direct pore loading determination

When evaluating the performance of an immobilized enzyme the comparison to free enzyme is often made. For an accurate comparison, the amount of both free and immobilized enzyme should be known. The amount of immobilized enzyme per amount of particles is usually reported as the weight of immobilized enzyme per mesoporous particle weight, the pore loading ( $P_{LD}$ ). The common method to determine pore loading is by indirect measurements. After the immobilization the particles are removed and the protein concentration in the surrounding solution is determined. The data are used to calculate the immobilized amount. In paper VII we explore the possibilities to do these measurements directly on the protein containing particles. The protein content could then be determined independent of monitoring of the immobilization. This could *e.g.* be useful to determine the protein content of particles recovered from a reaction. Due to leakage the measured content could be lower than the initial content after the immobilization.

In this study three methods for protein concentration determination (section 5.2) are examined for this purpose: Intrinsic absorption at 280 nm (section 5.2.1), the

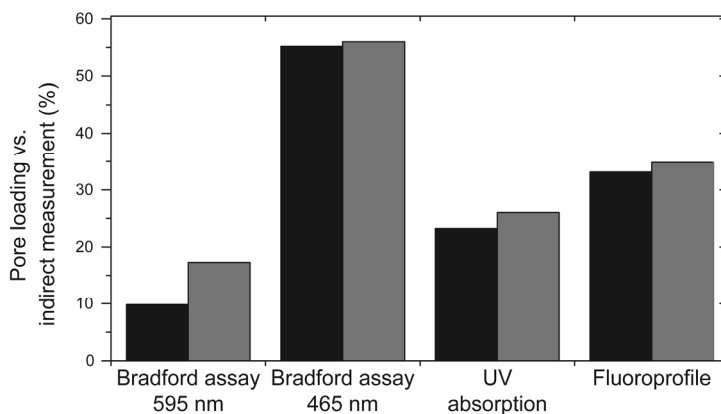


Figure 20 Pore loading determined by different direct methods compared to the pore loading determined indirectly represented in %. Indirectly determined pore loading is 100 µg/mg (black) or 60 µg/mg (grey) respectively. Data are from paper VII.

Bradford assay [154] (section 5.2.2), and a fluorescence based assay using the epicocconone dye [169] (section 5.2.3). In the absorption based methods correction for the light scattering caused by the suspended particles were applied (section 5.1.1). Some of the aspects of detection have been discussed above (section 7.1).

The protein signal can be seen to increase linearly with increasing particle concentration for a given set of particles both for 280 nm absorbance and for epicocconone fluorescence. There are also clear differences in protein signal for these methods seen for different sets of particles with different pore loading. For the measurements with the regular Bradford assay [154] no distinguishable concentration trends could be observed. This could be caused by either one or a combination of physic-chemical effects. It could either be interaction between Coomassie blue and the silica surface, reducing the amount of available dye molecules and thereby also the protein response, or unavailable binding sites on the protein due to binding to the silica. Absorption flattening will also be influencing the absorption signal. There is an adaptation of the Bradford assay described for immobilized proteins [220] based on measurements of the decrease of unbound dye as it binds to proteins in the solid material. This method shows a linear dependence between signal and particle concentration. The difference in pore loading can also be seen by this method.

Compared to indirect measurements, all methods used show a lower pore loading (Figure 20). The relative error between sets of particles with different pore loading is small for all methods except the regular Bradford assay. The difference in

response between the different methods are quite large and can not to date be fully explained. We suggest a combination of binding site availability, particle mass change, absorption flattening, correction procedure and increased quantum yield but cannot separate the effects.

Finally, we conclude that all methods examined, but the standard Bradford assay, could be used to determine the pore loading. The choice of method depends on the character of the sample. Intrinsic absorption at 280 nm is non-consuming and could be used for rare samples. The epicocconone assay is more sensitive and could be used for particles with lower pore loading. These techniques with the same considerations could also apply for enzymes attached to non-porous nanoparticles, which are utilized in widely separated fields such as electrochemical sensors and food processing.

### 7.3 Pore filling analysis

The pore loading  $P_{LD}$  (section 7.2) is not fully representative of the actual protein concentration in the pores as it is greatly influenced by variations in pore volume of the particles and the density differences between enzymes and the particles. In paper VIII, literature data on particles with immobilized enzyme are evaluated in terms of the pore filling,  $P_f$ . In equation 30 we define pore filling as the fraction of the pore volume which is occupied by the proteins (assuming that the enzymes are small enough to fit inside the pores)

$$P_f = \frac{V_{prot} \cdot N_{prot}}{V_{pore}} \quad (30)$$

where  $V_{prot}$  is the volume of each protein molecule,  $N_{prot}$  the number of proteins in each particle, and  $V_{pore}$  the total pore volume per particle. The number of proteins per particle,  $N_{prot}$ , can be calculated from the protein loading,  $P_{LD}$  using equation 31 where  $N_A$  is the Avogadro constant,  $M_{prot}$  is the protein molar mass and  $m_{part}$  the mass of a single particle.

$$N_{prot} = \frac{N_A \cdot P_{LD} \cdot m_{part}}{M_{prot}} \quad (31)$$

Equation 30 can be developed to contain the common material parameters particle specific pore volume,  $v_{pores}$  and the density,  $\rho_{solids}$  of the solid material in the pore walls, *e.g.* silica. The resulting equation (32) then becomes

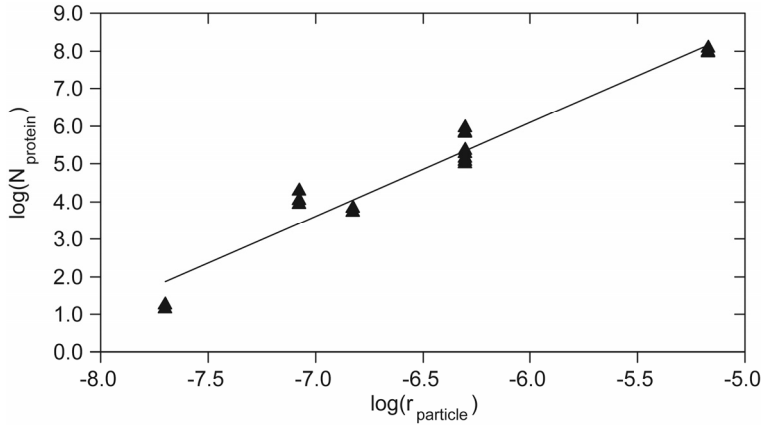


Figure 21 Double logarithmic plot of the number of immobilized enzyme molecules in particles of different sizes given as particle radius (metre) based on the data in paper VIII. The least-square linear fit yields a slope of 2.50 ± 0.01.

$$P_f = \frac{V_{prot} \cdot N_{prot} \cdot (v_{pore} + \rho_{solid}^{-1})}{V_{part} \cdot v_{pore}} \quad (32)$$

This equation can be used to calculate the pore filling from commonly available particle and protein data. The amount of protein that is adsorbed to the outer surface of the particles is here assumed to be negligible. This assumption is reasonable since the external surface typically only contributes to 1-2% of the total surface area. When the calculations indicate a pore filling of a few percent, care should be taken to prove that the enzymes really are located in the pores.

In paper VIII data from a large set of published studies where enzymes were immobilized in mesoporous silica particles were collected. The studies covered a wide range of proteins, particle sizes and pore sizes. The  $N_{prot}$  and the  $P_f$  were calculated using equations 31 and 32 assuming spherical particles and in most cases spherical proteins. The  $N_{prot}$  values are strongly affected by the particle size and cover almost seven orders of magnitude. The largest particles contain about  $10^8$  protein molecules while the smallest only contains slightly more than 10 molecules each. The number of protein molecules per particle was plotted against the radius of the particle in a log-log format in Figure 21 and the data were fitted to a linear model. The slope of this line can be connected to the filling mode of the particles. A slope of 2 is expected if the proteins only bind to the outer surface of the particles because the area scales as the radius squared, whereas a slope of 3 is expected if the proteins fill the pores in the

whole particle volume. The fact that the slope value is 2.5 in Figure 21 suggests an intermediate particle filling model. This slope value confirms that the proteins enter the pores (it is significantly larger than 2) but indicates that the full particle volumes is not equally occupied by enzymes (the slope is significantly lower than 3). The simplest model explaining this is that for steric reasons the proteins cannot enter all the pores. The pore volume measured may not be fully accessible to the proteins because of their larger size in comparison to *e.g.* N<sub>2</sub> used to determine the pore volume by adsorption.

The pore filling values calculated from literature data vary only by a factor of 10. This is considerably less than the values for  $N_{pms}$ , suggesting that the pores of particles of different sizes are filled with proteins to a similar extent. The calculations of pore filling based on using equation 32 may be compared with maximum values based on models for close packing of enzymes in pores. Ideal spherical enzymes can reach a maximum close packing of 67% in cylindrical pores ( $Pf = 0.67$ ) under optimal ratio between the dimension of the pore and the enzyme. All calculated values in paper VIII are lower than this caused by *e.g.* repelling protein-protein forces. It should be noted that the packing efficiency will be significantly reduced compared to close packing if the pore diameter is slightly larger than the enzyme dimensions.

The pore filling parameter describes the degree to which enzymes occupy the pores. This parameter can show how the pore volume is utilized and thereby be a relevant analysis tool. Optimal support materials could be identified by relating pore filling and immobilization efficiency. In analogy with the pore filling findings I here suggest the use of the corresponding term surface coverage as an analysis tool in studying enzyme immobilization onto non-porous particles. The surface coverage is relevant to evaluate the influence of both protein-protein interactions and protein-surface interactions that may affect the specific activity of immobilized enzymes.

## 7.4 Pore pH and pore microenvironment

As stated above in section 3 immobilization of enzymes into mesoporous particles has been shown to enhance enzyme stability, specific activity, and product selectivity [60]. This is probably due to both surface-enzyme interactions and the pore environment differing from bulk solution. The silica surface is expected to have a net negative charge above pH 2.7, the pI of the silanol groups. Changing the pH of the surrounding solution will alter the silica surface charge, but the surface charges are on the other hand likely to alter the pH close to the surface. The pH experienced by the immobilized enzymes may not be the same as measured in bulk solution. It

Table 4 pH monitored by BSA and FAE bound SNARF-1 immobilized in mesoporous silica particles

Bulk pH	SNARF-1 BSA		SNARF-1 FAE	
	Water		Butanol/water <sup>1</sup>	
6	6.5	6.4	n/a	6.4
7	7.1	7.0	6.5	7.0
8	7.7	7.7	n/a	7.5

Data from paper VI. <sup>1</sup> 92.5% 1-butanol and 7.5% water. Bulk pH refers to aqueous component before mixing.

was earlier seen that the immobilization was pH dependent [87] and more interestingly, that there seemed to be a difference in enzymatic activity between free and immobilized enzyme that are coupled to the altered pH in the pore environment [88, 221].

In this study (paper VI) the pH sensitive fluorescent dye SNARF-1 was used to determine the pH in mesoporous silica particles. SNARF-1 was covalently attached to BSA and a feruloyl esterase (FAE, the enzyme of [88]). Previous determination of pH in mesoporous silica was done using direct linking of a pH sensitive dye to an amine-functionalized surface [222]. The strategy in paper VI was chosen since the interesting environment *i.e.* where the enzyme was situated could be directly monitored. Further, the functionalization of the surface might change the chemical properties of the mesoporous silica and thereby the pH of the pores. As a result of these arguments we state that the method applied in paper VI is likely more relevant when studying protein immobilization.

The stained proteins were immobilized separately into mesoporous silica particles (diameter 1  $\mu\text{m}$ , pore diameter 7.8 nm) by physical adsorption. The protein loading was determined by supernatant absorbance to be 60  $\mu\text{g}/\text{mg}$  for BSA and 43  $\mu\text{g}/\text{mg}$  for FAE, respectively. The particles were washed and then dried under vacuum. The dry particles were dissolved in different pH-buffers and also in a solvent mixture of water and butanol, 7.5/92.5% by volume where the water fractions were different pH-buffers. The solvent mixture of butanol and water is a solution for the FAE transesterification reaction [88]. The emission spectrum of SNARF-1 consists of two peaks, where the relative amplitude changes with pH with a  $\text{pK}_a$  of 7.6 [223]. A calibration curve with the peak ratios was recorded using BSA in a wide range of pH-buffers.

The method of using SNARF-1 as a pH reporter molecule was verified in the protein bound mesoporous silica particle context. The covalent attachment of SNARF-1 to BSA or FAE does not change the pH dependence of the emission peak ratio. The spectral shape of the immobilized SNARF-1-protein complex emission was not visibly altered. This statement does not include the peak ratio because it is the reporter of pH. The spectra measured on samples of immobilized protein could be interpreted as pH signals. When the particles were dispersed in pure pH buffers the pore pH was found to be more neutral than in bulk solution (Table 4). This suggests that the silica pore contains a buffering agent that is active in the range close to neutral. The silanol groups are known to have a  $pK_a$  at 2.7 but the silica surfaces may also contain a second type of silanol site with a  $pK_a$  of about 8.5 [224]. Together these types of silanol groups may buffer the pH in the pore in the range 6-8.

When the particles were suspended in the butanol/water mixture the reported pH was similar to the one when dispersed in pure pH buffers (Table 4). However, when the proteins were dissolved in the solvent mixture without the particles present the SNARF-1 emission spectra were distinctly different. The spectra were blue-shifted, almost resembling the low pH form of SNARF-1, at all pH measured. This is not due to a low pH in these solutions but to a solvatochromic effect of the organic solvent present. These results show that the pore environment is clearly different from the one experienced by the protein in solution. No difference in net solvent composition could be measured, but the observed spectral difference may be caused by the solvent organisation in the pores.

## 8 Concluding remarks

A large portion of the work that is the basis of this thesis has centred on the spectroscopic issues of complex samples. Do you get the same spectroscopic response in a particle or a bilayer environment as you would in dilute solution? Although not being the key objective of each study this has been a central consideration in the design of the experiments. There are several spectroscopic artefacts that can appear as a result of the sample composition. What sometimes is an unwanted artefact could in other cases be the spectroscopic response needed to confirm a hypothesis. It is important to be aware of the pitfalls when using spectroscopic assays in these complex samples.

We have seen spectral changes of dyes coupled to the solvent environment were the molecules are found. Examples of this have been seen *e.g.* with different solvents in paper V and the solvent mixture in paper VI. We have seen molecular interactions such as dimer formation of voltage sensitive dyes in paper V, end-stacking of cyanine dyes and DNA in paper III, and the ion-pair formation of ATOTA in paper IV all causing spectral shifts or changes in spectral shapes. Commonly applied interpretation of spectroscopic data, *e.g.* the Beer-Lambert law (equation 11), assumes the sample to be a dilute, homogenous, and isotropic solution. An anisotropic sample will have different absorbance depending on the grazing angle. This phenomenon has been utilized in paper III in the LD experiments, but at the same time in paper III the absorption data had to be corrected for the anisotropy. When particles are present in the spectroscopic sample there will be light scattering. In paper VII (and paper X) the correction for such light scattering absorbance signal is a central part. In principle it is observed that the light scattering and absorption are additive signals and therefore could be separated. When the absorbing species is located unevenly in the sample, which is the case with immobilized enzymes in mesoporous particles, the absorption flattening (equation 19) has to be considered. In paper VII this effect was considered small due to low total absorption by the particles.

So far the spectroscopic effects of the confinement and the complexity of the samples. Switching to the biophysical effects, effects of both surfaces and confinement have been studied. The biomolecule-ligand interactions may be altered in a surface rich environment in comparison to a bulk solution. The normally strong DNA intercalators examined in paper III do not intercalate in presence of the charged bilayer surfaces of a lamellar liquid crystal but instead bind to the surface. Similarly, the end-stacking of Cy5 covalently attached to DNA was disfavoured for

surface binding in the same manner when there were charged bilayer surfaces present. In papers VI and VII the enzyme immobilization is caused by the interactions between the enzyme and the silica surface. Although the nature of these interactions was not studied in this thesis they are the basis of non-covalent immobilization. Some ongoing studies not included in this thesis concern the rate and as a consequence also the mechanism of immobilization. The size of the enzyme in relation to the size of the pores gives rise to differences in immobilization rate. By recording changes in fluorescence over time the immobilization process can be monitored and this data can also be used to evaluate models of the immobilization process. This can hopefully help to further understand the process of immobilizing enzymes into mesoporous particles.

The confinement of biomolecules into small volumes not vastly larger than the molecules themselves gives rise to special effects. In this thesis this has *e.g.* been seen in paper III as the orientation of oligonucleotides in the aqueous interstitia of a lamellar liquid crystal. The thin water layers between lipid bilayers restrict the movement of the rod-like molecule to the plane perpendicular to the bilayer normal. The available volume between the surfaces is thinner than the length of the oligonucleotide and that forces it to move mainly in only two dimensions. The narrow environment of liquid crystals was also utilized in papers I and II to separate oligonucleotides by electrophoresis based on size and conformation. The water channels of the cubic liquid crystal are nanometer sized, just like the oligonucleotides that were studied. This caused a strong retardation and thereby slow migration when subjected to an electric field. The effect on immobilized enzymes by the confinement into narrow pores is central for the field of mesoporous biocatalysts. This effect has not been studied in this thesis, but has been a motivation for studying these systems. The complexity of these particle systems has been the motivation for another ongoing investigation. There is no information on the homogeneity of the particle population. The techniques used in this thesis reports on average properties of a population of particles with immobilized enzyme. It is therefore interesting to develop techniques to study how *e.g.* the pore loading varies in a particle population and how measurements on single particles compare to bulk measurements.

## 9 Acknowledgements

I would like to take the opportunity to thank my supervisor Björn Åkerman for giving me the opportunity to work in this project. You have given me the freedom to pursue research in the directions curiosity has led me. It is a great joy to work together with you.

This work has been done as a part of the Linnaeus Centre for bio-inspired supramolecular function and design, SUPRA. I especially thank the members of the SUPRA cluster “Enzyme-catalysed reactions in confined media”: Christian Thörn, Hanna Gustafsson, Lisbeth Olsson and Krister Holmberg for nice discussions and collaboration.

Further, I would like to thank my co-supervisors Anette Larsson and Krister for all your support.

I am thankful to all my co-authors, especially Annika, Catherine, Fabian, Hanna, Fredrik, Maria and those mentioned above. Without your support and cooperation this work would not have been done.

I thank my current project collaborators for their patience. Hopefully I will return to our projects with more intensity after completing this thesis.

Past and present colleagues are acknowledged for creating a enjoyable and inspiring atmosphere. I am especially thankful to Pär for his involvement in my return to physical chemistry.

The floor ball group of physical chemistry has been helpful in my futile efforts to at least partly slowing down the physical deterioration.

Last but definitely not least, I would like to thank Liza for putting up with my long work days during writing, for helping me proof reading and of course for all your love.

## 10 References

1. Whitesides, G.M., J.K. Kriebel, and B.T. Mayers, Self-Assembly and Nanostructured Materials, in *Nanoscale Assembly: Chemical Techniques*, W.T.S. Huck, Editor. 2005, Springer.
2. Whitesides, G.M. and M. Boncheva, Beyond molecules: Self-assembly of mesoscopic and macroscopic components. *Proc. Natl. Acad. Sci. U. S. A.*, 2002. **99**(8): p. 4769-4774.
3. Eicke, H.-F., Surfactants in nonpolar solvents, in *Micelles*. 1980, Springer. p. 85-145.
4. Jones, E.R. and C.R. Bury, The freezing-points of concentrated solutions. — Part II. Solutions of formic, acetic, propionic, and butyric acids. *Philos. Mag.*, 1927. **4**(23): p. 841-848.
5. Ekwall, P., Om ytaktiviteten hos lösningar av högmolekylära fettsyroras natriumsalter. *Acta Acad. Abo., Math. Phys.*, 1927. **4**(6): p. 3-209.
6. Grindley, J. and C.R. Bury, The densities of butyric acid-water mixtures. *J. Chem. Soc.*, 1929: p. 679-684.
7. Lottemoser, A. and F. Püschel, Leitfähigkeits- und Potentialmessungen an Salzen der höheren Alkylschwefelsäuren. *Kolloid Z.*, 1933. **63**(2): p. 175-192.
8. McBain, T.W., E.C.V. Cornish, and R.C. Bowden, Studies of the constitution of soap in solution sodium myristate and sodium laurate. *J. Chem. Soc., Trans.*, 1912. **101**: p. 2042-2056.
9. McBain, J.W., Mobility of highly-charged micelles. *Trans. Faraday Soc.*, 1913. **9**: p. 99-101.
10. Israelachvili, J.N., D.J. Mitchell, and B.W. Ninham, Theory of self-assembly of hydrocarbon amphiphiles into micelles and bilayers. *J. Chem. Soc. Farad. T. 2*, 1976. **72**: p. 1525-1568.
11. Luzzati, V., H. Mustacchi, and A. Skoulios, The structure of the liquid-crystal phases of some soap + water systems. *Discuss. Faraday Soc.*, 1958. **25**(0): p. 43-50.
12. Fontell, K., Cubic phases in surfactant and surfactant-like lipid systems. *Colloid Polym. Sci.*, 1990. **268**(3): p. 264-285.
13. Luzzati, V., H. Mustacchi, and A. Skoulios, Structure of the liquid-crystal phases of the soap-water system: Middle soap and neat soap. *Nature*, 1957. **180**(4586): p. 600-6001.

14. McBain, J.W. and S.S. Marsden, The structural types of aqueous systems of surface-active substances and their X-ray diffraction characteristics. *Acta Cryst.*, 1948. **1**(5): p. 270-272.
15. Marsden, S.S. and J.W. McBain, Aqueous systems of non-ionic detergents as studied by X-ray diffraction. *J. Phys. Colloid Chem.*, 1948. **52**(1): p. 110-130.
16. Hyde, S.T., Identification of lyotropic liquid crystalline mesophases, in *Handbook of Applied Surface and Colloid Chemistry*, K. Holmberg, Editor. 2001, J. Wiley & Sons. p. 299-332.
17. Schwartz, H.A., *Gesammelte matematische Abhandlungen*. Vol. 1. 1890: Springer.
18. Fontell, K., Some aspects on the cubic phases in surfactant and surfactant-like lipid systems. *Adv. Colloid Interface Sci.*, 1992. **41**: p. 127-147.
19. Rummel, G., A. Hardmeyer, C. Widmer, M.L. Chiu, P. Nollert, K.P. Locher, I. Pedruzzi, E.M. Landau, and J.P. Rosenbusch, Lipidic cubic phases: New matrices for the three-dimensional crystallization of membrane proteins. *J. Struct. Biol.*, 1998. **121**(2): p. 82-91.
20. Schoen, A.H., Infinite regular warped polyhedra and infinite periodic minimal surfaces. *Not. Am. Math. Soc.*, 1968. **15**: p. 727.
21. Schoen, A.H., A fifth intersection-free infinite periodic minimal surface (IPMS) of cubic symmetry. Preliminary report. *Not. Am. Math. Soc.*, 1969. **16**(3): p. 519.
22. Schoen, A.H. *Infinite peridic minimal surfaces without self-intersections*. 1970, NASA TN D-5541
23. Hyde, S.T., Microstructure of bicontinuous surfactant aggregates. *J. Phys. Chem.*, 1989. **93**(4): p. 1458-1464.
24. Aota-Nakano, U., S.J. Li, and M. Yamazaki, Effects of electrostatic interaction on the phase stability and structures of cubic phases of monoolein/oleic acid mixture membranes. *Biochim. Biophys. Acta, Biomembr.*, 1999. **1461**(1): p. 96-102.
25. Zhao, D.Y., J.L. Feng, Q.S. Huo, N. Melosh, G.H. Fredrickson, B.F. Chmelka, and G.D. Stucky, Triblock copolymer syntheses of mesoporous silica with periodic 50 to 300 Angstrom pores. *Science*, 1998. **279**(5350): p. 548-552.
26. Zhao, D.Y., Q.S. Huo, J.L. Feng, B.F. Chmelka, and G.D. Stucky, Nonionic triblock and star diblock copolymer and oligomeric surfactant syntheses of highly ordered, hydrothermally stable, mesoporous silica structures. *J. Am. Chem. Soc.*, 1998. **120**(24): p. 6024-6036.

27. Svingen, R., P. Alexandridis, and B. Åkerman, On the mechanism of electrophoretic migration of DNA in pluronic gels. *Langmuir*, 2002. **18**(22): p. 8616-8619.
28. Svingen, R. and B. Åkerman, Mechanism of electrophoretic migration of DNA in the cubic phase of pluronic F127 and water. *J. Phys. Chem. B*, 2004. **108**(8): p. 2735-2743.
29. Hoar, T.P. and J.H. Schulman, Transparent water-in-oil dispersions the oleopathic hydro-micelle. *Nature*, 1943. **152**: p. 102-103.
30. Gazeau, D., A.M. Bellocq, D. Roux, and T. Zemb, Experimental evidence for random surface structures in dilute surfactant solutions. *Europhys. Lett.*, 1989. **9**(5): p. 447.
31. Bangham, A.D. and R.W. Horne, Negative staining of phospholipids and their structural modification by surface-active agents as observed in the electron microscope. *J. Mol. Biol.*, 1964. **8**(5): p. 660 - IN610.
32. Brian, A.A. and H.M. McConnell, Allogenic stimulation of cytotoxic T cells by supported planar membranes. *Proc. Natl. Acad. Sci. U. S. A.*, 1984. **81**(19): p. 6159-6163.
33. Richter, R.P., R. Berat, and A.R. Brisson, Formation of solid-supported lipid bilayers: An integrated view. *Langmuir*, 2006. **22**(8): p. 3497-3505.
34. Sackmann, E., Physical basis of self-organization and function of membranes: Physics of vesicles, in *Handbook of biological physics*, R. Lipowsky and E. Sackmann, Editors. 1995, Elsevier Science B.V. p. 213-303.
35. Sankaram, M.B., D. Marsh, and T.E. Thompson, Estimation of gel and fluid domain sizes in two-component lipid bilayers, in *The structure and conformation of amphiphilic membranes*, R. Lipowsky, D. Richter, and K. Kremer, Editors. 1992, Springer. p. 45-48.
36. Marder, M., H.L. Frisch, J.S. Langer, and H.M. McConnell, Theory of the intermediate rippled phase of phospholipid bilayers. *Proc. Natl. Acad. Sci. U. S. A.*, 1984. **81**(20): p. 6559-6561.
37. Morrow, M.R., J.P. Whitehead, and D. Lu, Chain-length dependence of lipid bilayer properties near the liquid crystal to gel phase transition. *Biophys. J.*, 1992. **63**(1): p. 18-27.
38. Nagle, J.F., Theory of lipid monolayer and bilayer phase transitions: Effect of headgroup interactions. *J. Membr. Biol.*, 1976. **27**(1): p. 233-250.
39. Evans, E. and D. Needham, Physical properties of surfactant bilayer membranes: Thermal transitions, elasticity, rigidity, cohesion, and colloidal interactions. *J. Phys. Chem.*, 1987. **91**(16): p. 4219-4228.

40. Rawicz, W., K.C. Olbrich, T. McIntosh, D. Needham, and E. Evans, Effect of chain length and unsaturation on elasticity of lipid bilayers. *Biophys. J.*, 2000. **79**(1): p. 328 - 339.
41. Singer, S.J. and G.L. Nicolson, The fluid mosaic model of the structure of cell membranes. *Science*, 1972. **175**(4023): p. 720-731.
42. Luzzati, V., Biological significance of lipid polymorphism: the cubic phases - Commentary. *Curr. Opin. Struc. Biol.*, 1997. **7**(5): p. 661-668.
43. Kulkarni, C.V., O. Ces, R.H. Templer, and J.M. Seddon, Pressure effects on a protein-lipid model membrane. *Soft Matter*, 2013. **9**(28): p. 6525-6531.
44. Larsson, K., Cubic lipid-water phases: Structures and biomembrane aspects. *J. Phys. Chem.*, 1989. **93**(21): p. 7304-7314.
45. Mueller, P., D.O. Rudin, H.T. Tien, and W.C. Wescott, Reconstitution of cell membrane structure *in vitro* and its transformation into an excitable system. *Nature*, 1962. **194**(4832): p. 979-980.
46. Armstrong, C.M. and B. Hille, Voltage-gated ion channels and electrical excitability. *Neuron*, 1998. **20**(3): p. 371-380.
47. Reimhult, E., F. Höök, and B. Kasemo, Intact vesicle adsorption and supported biomembrane formation from vesicles in solution: Influence of surface chemistry, vesicle size, temperature, and osmotic pressure. *Langmuir*, 2003. **19**(5): p. 1681-1691.
48. Kalb, E., S. Frey, and L.K. Tamm, Formation of supported planar bilayers by fusion of vesicles to supported phospholipid monolayers. *Biochim. Biophys. Acta, Biomembr.*, 1992. **1103**(2): p. 307 - 316.
49. Salamon, Z., Y. Wang, G. Tollin, and H.A. Macleod, Assembly and molecular organization of self-assembled lipid bilayers on solid substrates monitored by surface plasmon resonance spectroscopy. *Biochim. Biophys. Acta, Biomembr.*, 1994. **1195**(2): p. 267-275.
50. Gabriel, N.E. and M.F. Roberts, Spontaneous formation of stable unilamellar vesicles. *Biochemistry*, 1984. **23**(18): p. 4011-4015.
51. Sanders, C.R. and G.C. Landis, Facile acquisition and assignment of oriented sample NMR spectra for bilayer surface-associated proteins. *J. Am. Chem. Soc.*, 1994. **116**(14): p. 6470-6471.
52. Sanders, C.R. and G.C. Landis, Reconstitution of membrane proteins into lipid-rich bilayered mixed micelles for NMR studies. *Biochemistry*, 1995. **34**(12): p. 4030-4040.
53. Kogan, M., T. Beke-Somfai, and B. Nordén, Flow-alignment of bicellar lipid mixtures: orientations of probe molecules and membrane-associated biomacromolecules in lipid membranes studied with polarized light. *Chem. Commun.*, 2011. **47**(26): p. 7356-7358.

54. Papahadjopoulos, D. and N. Miller, Phospholipid model membranes I. Structural characteristics of hydrated liquid crystals. *Biochim. Biophys. Acta*, 1967. **135**(4): p. 624-638.
55. Papahadjopoulos, D. and J.C. Watkins, Phospholipid model membranes II. Permeability properties of hydrated liquid crystals. *Biochim. Biophys. Acta*, 1967. **135**(4): p. 639-652.
56. Wiener, M.C. and S.H. White, Structure of a fluid dioleoylphosphatidylcholine bilayer determined by joint refinement of X-ray and neutron diffraction data: III. Complete structure. *Biophys. J.*, 1992. **61**(2 J): p. 434-447.
57. Caboi, F., G.S. Amico, P. Pitzalis, M. Monduzzi, T. Nylander, and K. Larsson, Addition of hydrophilic and lipophilic compounds of biological relevance to the monoolein/water system. I. Phase behavior. *Chem. Phys. Lipids*, 2001. **109**(1): p. 47-62.
58. Toraya, S., T. Nagao, K. Norisada, S. Tuzi, H. Saitô, S. Izumi, and A. Naito, Morphological behavior of lipid bilayers induced by melittin near the phase transition temperature. *Biophys. J.*, 2005. **89**(5): p. 3214-3222.
59. Hianik, T., V.A. Buckin, and B. Piknova, Can a single Bacteriorhodopsin molecule change the structural state of one liposome? *Gen. Physiol. Biophys.*, 1994. **13**(6): p. 493-501.
60. Hudson, S., J. Cooney, and E. Magner, Proteins in mesoporous silicates. *Angew. Chem., Int. Ed.*, 2008. **47**(45): p. 8582-8594.
61. Rosenholm, J.M., V. Mamaeva, C. Sahlgren, and M. Linden, Nanoparticles in targeted cancer therapy: mesoporous silica nanoparticles entering preclinical development stage. *Nanomedicine*, 2012. **7**(1): p. 111-120.
62. Slowing, I.I., J.L. Vivero-Escoto, C.-W. Wu, and V.S.Y. Lin, Mesoporous silica nanoparticles as controlled release drug delivery and gene transfection carriers. *Adv. Drug Deliv. Rev.*, 2008. **60**(11): p. 1278-1288.
63. Lee, C.-H., T.-S. Lin, and C.-Y. Mou, Mesoporous materials for encapsulating enzymes. *Nano Today*, 2009. **4**(2): p. 165-179.
64. Hudson, S., E. Magner, J. Cooney, and B.K. Hodnett, Methodology for the immobilization of enzymes onto mesoporous materials. *J. Phys. Chem. B*, 2005. **109**(41): p. 19496-19506.
65. Rouquerol, J., D. Avnir, C.W. Fairbridge, D.H. Everett, J.H. Haynes, N. Pernicone, J.D.F. Ramsay, K.S.W. Sing, and K.K. Unger, Recommendations for the characterization of porous solids. *Pure Appl. Chem.*, 1994. **66**(8): p. 1739-1758.

66. Yang, P.D., D.Y. Zhao, D.I. Margolese, B.F. Chmelka, and G.D. Stucky, Generalized syntheses of large-pore mesoporous metal oxides with semicrystalline frameworks. *Nature*, 1998. **396**(6707): p. 152-155.
67. Bagshaw, S.A. and T.J. Pinnavaia, Mesoporous alumina molecular sieves. *Angew. Chem., Int. Ed.*, 1996. **35**(10): p. 1102-1105.
68. Bagshaw, S.A., E. Prouzet, and T.J. Pinnavaia, Templating of mesoporous molecular sieves by nonionic polyethylene oxide surfactants. *Science*, 1995. **269**(5228): p. 1242-1244.
69. Antonelli, D.M. and J.Y. Ying, Synthesis of hexagonally packed mesoporous TiO<sub>2</sub> by a modified sol-gel method. *Angew. Chem., Int. Ed.*, 1995. **34**(18): p. 2014-2017.
70. Zhang, R., A.A. Elzatahry, S.S. Al-Deyab, and D. Zhao, Mesoporous titania: From synthesis to application. *Nano Today*, 2012. **7**(4): p. 344-366.
71. Beck, J.S., J.C. Vartuli, W.J. Roth, M.E. Leonowicz, C.T. Kresge, K.D. Schmitt, C.T.W. Chu, D.H. Olson, and E.W. Sheppard, A new family of mesoporous molecular sieves prepared with liquid crystal templates. *J. Am. Chem. Soc.*, 1992. **114**(27): p. 10834-10843.
72. Kresge, C.T., M.E. Leonowicz, W.J. Roth, J.C. Vartuli, and J.S. Beck, Ordered mesoporous molecular sieves synthesized by a liquid-crystal template mechanism. *Nature*, 1992. **359**(6397): p. 710-712.
73. Vartuli, J.C., K.D. Schmitt, C.T. Kresge, W.J. Roth, M.E. Leonowicz, S.B. Mccullen, S.D. Hellring, J.S. Beck, J.L. Schlenker, D.H. Olson, and E.W. Sheppard, Effect of surfactant silica molar ratios on the formation of mesoporous molecular sieves: Inorganic mimicry of surfactant liquid-crystal phases and mechanistic implications. *Chem. Mater.*, 1994. **6**(12): p. 2317-2326.
74. Sanchez, C., C. Boissière, D. Grosso, C. Laberty, and L. Nicole, Design, synthesis, and properties of inorganic and hybrid thin films having periodically organized nanoporosity. *Chem. Mater.*, 2008. **20**(3): p. 682-737.
75. Ciesla, U. and F. Schüth, Ordered mesoporous materials. *Microporous Mesoporous Mater.*, 1999. **27**(2-3): p. 131-149.
76. Tolbert, S.H., A. Firouzi, G.D. Stucky, and B.F. Chmelka, Magnetic field alignment of ordered silicate-surfactant composites and mesoporous silica. *Science*, 1997. **278**(5336): p. 264-268.
77. Alfredsson, V., M.W. Anderson, T. Ohsuna, O. Terasaki, M. Jacob, and M. Bojrup, Cubosome description of the inorganic mesoporous structure MCM-48. *Chem. Mater.*, 1997. **9**(10): p. 2066-2070.
78. Rouquerol, F., J. Rouquerol, and K. Sing, *Adsorption by powders and porous solids*. 1999: Academic press.

79. Brunauer, S., P.H. Emmett, and E. Teller, Adsorption of gases in multimolecular layers. *J. Am. Chem. Soc.*, 1938. **60**: p. 309-319.
80. Stein, A., B.J. Melde, and R.C. Schroden, Hybrid inorganic–organic mesoporous silicates—Nanoscope reactors coming of age. *Adv. Mater.*, 2000. **12**(19): p. 1403-1419.
81. Melde, B.J., B.J. Johnson, and P.T. Charles, Mesoporous silicate materials in sensing. *Sensors*, 2008. **8**(8): p. 5202-5228.
82. Descalzo, A.B., M. Dolores Marcos, C. Monte, R. Martínez-Máñez, and K. Rurack, Mesoporous silica materials with covalently anchored phenoxazinone dyes as fluorescent hybrid materials for vapour sensing. *J. Mater. Chem.*, 2007. **17**(44): p. 4716-4723.
83. Li, L.-L., H. Sun, C.-J. Fang, J. Xu, J.-Y. Jin, and C.-H. Yan, Optical sensors based on functionalized mesoporous silica SBA-15 for the detection of multianalytes ( $H^+$  and  $Cu^{2+}$ ) in water. *J. Mater. Chem.*, 2007. **17**(42): p. 4492-4498.
84. Malvi, B. and S. Sen Gupta, Encapsulation of enzyme in large mesoporous material with small mesoporous windows. *Chem. Commun.*, 2012. **48**(63): p. 7853-7855.
85. He, J., X. Li, D.G. Evans, X. Duan, and C. Li, A new support for the immobilization of penicillin acylase. *J. Mol. Catal. B: Enzym.*, 2000. **11**(1): p. 45-53.
86. Reis, P., T. Witula, and K. Holmberg, Mesoporous materials as host for an entrapped enzyme. *Microporous Mesoporous Mater.*, 2008. **110**(2-3): p. 355-362.
87. Gustafsson, H., C. Thörn, and K. Holmberg, A comparison of lipase and trypsin encapsulated in mesoporous materials with varying pore sizes and pH conditions. *Colloids Surf, B*, 2011. **87**(2): p. 464-471.
88. Thörn, C., H. Gustafsson, and L. Olsson, Immobilization of feruloyl esterases in mesoporous materials leads to improved transesterification yield. *J. Mol. Catal. B: Enzym.*, 2011. **72**(1-2): p. 57-64.
89. Gustafsson, H., E.M. Johansson, A. Barrabino, M. Odén, and K. Holmberg, Immobilization of lipase from *Mucor miebei* and *Rhizopus oryzae* into mesoporous silica-The effect of varied particle size and morphology. *Colloids Surf, B*, 2012. **100**: p. 22-30.
90. Piras, M., A. Salis, M. Piludu, D. Steri, and M. Monduzzi, 3D vision of human lysozyme adsorbed onto a SBA-15 nanostructured matrix. *Chem. Commun.*, 2011. **47**(26): p. 7338-7340.
91. Suh, C.W., M.Y. Kim, J.B. Choo, J.K. Kim, H.K. Kim, and E.K. Lee, Analysis of protein adsorption characteristics to nano-pore silica particles

- by using confocal laser scanning microscopy. *J. Biotechnol.*, 2004. **112**(3): p. 267-277.
92. Matsuura, S.-i., R. Ishii, T. Itoh, T. Hanaoka, S. Hamakawa, T. Tsunoda, and F. Mizukami, Direct visualization of hetero-enzyme co-encapsulated in mesoporous silicas. *Microporous Mesoporous Mater.*, 2010. **127**(1-2): p. 61-66.
  93. Matsuura, S.-i., T. Itoh, R. Ishii, K. Sakaguchi, T. Tsunoda, T. Hanaoka, and F. Mizukami, The ensemble of hetero-proteins in inorganic nanochannels. *Bioconjugate Chem.*, 2008. **19**(1): p. 10-14.
  94. Matsuura, S.-i., T. Itoh, R. Ishii, T. Tsunoda, K. Sakaguchi, T. Hanaoka, and F. Mizukami, Encapsulation of fluorescent proteins in folded-sheet mesoporous materials: Effect of pore size on energy-transfer efficiency. *Microporous Mesoporous Mater.*, 2010. **131**(1-3): p. 245-251.
  95. de Broglie, L., A tentative theory of light quanta. *Philos. Mag.*, 1924. **47**(278): p. 446-458.
  96. Hecht, E., *Optics (4th Edition)*. 2001: Addison Wesley.
  97. Bohr, N., On the constitution of atoms and molecules. *Philos. Mag.*, 1913. **26**(151): p. 1-25.
  98. Jabłoński, A., Efficiency of anti-Stokes fluorescence in dyes. *Nature*, 1933. **131**: p. 839-840.
  99. Kasha, M., Characterization of electronic transitions in complex molecules. *Discuss. Faraday Soc.*, 1950(9): p. 14-19.
  100. Stokes, G.G., On the change of refrangibility of light. *Philos. T. R. Soc. Lond.*, 1852. **142**: p. 463-562.
  101. Kirk, W., Solvent Stokes' shifts revisited: Application and comparison of Thompson-Schweizer-Chandler-Song-Marcus theories with Ooshika-Bakshiev-Lippert theories. *J. Phys. Chem. A*, 2008. **112**(51): p. 13609-13621.
  102. Stevens, B. and E. Hutton, Radiative life-time of the Pyrene dimer and the possible role of excited dimers in energy transfer processes. *Nature*, 1960. **186**(4730): p. 1045-1046.
  103. Birks, J.B., Excimers. *Rep. Prog. Phys.*, 1975. **38**(8): p. 903-974.
  104. Dexter, D.L., A theory of sensitized luminescence in solids. *J. Chem. Phys.*, 1953. **21**(5): p. 836-850.
  105. Förster, T., Zwischenmolekulare Energiewanderung und Fluoreszenz. *Ann. Phys.*, 1948. **437**(1-2): p. 55-75.
  106. Thomson, J.J., On the number of corpuscles in an atom. *Philos. Mag.*, 1906. **11**(66): p. 769-781.

107. Compton, A.H., A quantum theory of the scattering of X-rays by light elements. *Phys. Rev.*, 1923. **21**(5): p. 0483-0502.
108. Strutt (Lord Rayleigh), J.W., On the scattering of light by small particles. *Philos. Mag.*, 1871. **41**(275): p. 447 - 454.
109. Mie, G., Beiträge zur Optik trüber Medien, speziell kolloidaler Metallösungen. *Ann. Phys.*, 1908. **330**(3): p. 377-445.
110. Jöbst, G., Diffuse Strahlung dielektrischer Kugeln im Grenzfalle, daß Kugelmaterial und umgebendes Medium fast gleiche Brechungsindices haben. *Ann. Phys.*, 1925. **383**(18): p. 157-166.
111. Lord Rayleigh, On the electromagnetic theory of light. *Philos. Mag.*, 1881(12).
112. Gans, R., Strahlungsdiagramme ultramikroskopischer Teilchen. *Ann. Phys.*, 1925. **381**(1): p. 29-38.
113. Koch, A.L., Some calculations on the turbidity of mitochondria and bacteria. *Biochim. Biophys. Acta*, 1961. **51**(3): p. 429-441.
114. Penney, C.M., Light scattering in terms of oscillator strengths and refractive indices. *J. Opt. Soc. Am.*, 1969. **59**(1): p. 34-&.
115. Raman, C.V. and K.S. Krishnan, A new type of secondary radiation. *Nature*, 1928. **121**: p. 501-502.
116. Raman, C.V. and K.S. Krishnan, A new class of spectra due to secondary radiation, Part I. *Indian J. Phys.*, 1928. **2**: p. 399-419.
117. Leach, S.J. and H.A. Scheraga, Effect of light scattering on ultraviolet difference spectra. *J. Am. Chem. Soc.*, 1960. **82**(18): p. 4790-4792.
118. Winder, A.F. and W.L.G. Gent, Correction of light-scattering errors in spectrophotometric protein determinations. *Biopolymers*, 1971. **10**(7): p. 1243-1251.
119. Duysens, L.N.M., The flattening of the absorption spectrum of suspensions, as compared to that of solutions. *Biochim. Biophys. Acta*, 1956. **19**: p. 1-12.
120. Wittung, P., J. Kajanus, M. Kubista, and B.G. Malmström, Absorption flattening in the optical spectra of liposome-entrapped substances. *FEBS Lett.*, 1994. **352**(1): p. 37-40.
121. Bustamante, C. and M.F. Maestre, Statistical effects in the absorption and optical activity of particulate suspensions. *Proc. Natl. Acad. Sci. U. S. A.*, 1988. **85**(22): p. 8482-8486.
122. Halling, P.J., Estimation of flattening coefficient for absorption and circular dichroism using simulation. *Anal. Biochem.*, 2009. **387**(1): p. 76-81.
123. Naqvi, K.R., T.B. Melo, B.B. Raju, T. Javorfi, and G. Garab, Comparison of the absorption spectra of trimers and aggregates of chlorophyll a/b light-

- harvesting complex LHC II. Spectroc. Acta Pt. A-Molec. Biomolec. Spectr., 1997. **53**(11): p. 1925-1936.
124. Gordon, D.J. and Holzwart, G., Artifacts in measured optical activity of membrane suspensions. Arch. Biochem. Biophys., 1971. **142**(2): p. 481-488.
  125. Urry, D.W., Protein conformation in biomembranes - optical rotation and absorption of membrane suspensions. Biochim. Biophys. Acta, 1972. **265**(1): p. 115-168.
  126. Latimer, P., The deconvolution of absorption spectra of green plant materials - improved corrections for the sieve effect. Photochem. Photobiol., 1983. **38**(6): p. 731-734.
  127. Jabłoński, A., Self-depolarization and decay of photoluminescence of solutions. Acta Phys. Pol., 1955. **14**: p. 295-307.
  128. Jabłoński, A., Decay of photoluminescence of solutions. Acta Phys. Pol., 1957. **16**: p. 471-479.
  129. Stryer, L. and R.P. Haugland, Energy transfer: a spectroscopic ruler. Proc. Natl. Acad. Sci. U. S. A., 1967. **58**(2): p. 719-726.
  130. Nordén, B., A. Rodger, and T.R. Dafforn, *Linear dichroism and circular dichroism - a textbook on polarized-light spectroscopy*. 2010: RSC Publishing.
  131. Wada, A., Chain regularity and flow dichroism of deoxyribonucleic acids in solution. Biopolymers, 1964. **2**(4): p. 361-380.
  132. Wada, A. and S. Kozawa, Instrument for studies of differential flow dichroism of polymer solutions. J. Polym. Sci. A, 1964. **2**(2PA): p. 853-864.
  133. Breton, J., Michelvi, M., and Pailloti, G., Orientation of pigments and structural proteins in photosynthetic membrane of spinach chloroplasts: A linear dichroism study. Biochim. Biophys. Acta, 1973. **314**(1): p. 42-56.
  134. Åkerman, B., M. Jonsson, and B. Nordén, Electrophoretic orientation of DNA detected by linear dichroism spectroscopy. J. Chem. Soc., Chem. Commun., 1985(7): p. 422-423.
  135. Jabłoński, A., Polarised photoluminescence of adsorbed molecules of dyes. Nature, 1934. **133**: p. 140-140.
  136. Nordén, B., G. Lindblom, and I. Jonáš, Linear dichroism spectroscopy as a tool for studying molecular orientation in model membrane systems. J. Phys. Chem., 1977. **81**(22): p. 2086-2093.
  137. Fujitani, Y., Small deformation of a liposome in a linear shear flow. Fluid Dyn. Res., 1995. **15**(1): p. 1.
  138. Kraus, M., W. Wintz, U. Seifert, and R. Lipowsky, Fluid vesicles in shear flow. Phys. Rev. Lett., 1996. **77**(17): p. 3685.

139. Ardhammar, M., N. Mikati, and B. Nordén, Chromophore orientation in liposome membranes probed with flow dichroism. *J. Am. Chem. Soc.*, 1998. **120**(38): p. 9957-9958.
140. Gårding, L. and B. Nordén, Simple formulas for rotation averages of spectroscopic intensities. *Chem. Phys.*, 1979. **41**(3): p. 431-437.
141. Ardhammar, M., P. Lincoln, and B. Nordén, Invisible liposomes: Refractive index matching with sucrose enables flow dichroism assessment of peptide orientation in lipid vesicle membrane. *Proc. Natl. Acad. Sci. U. S. A.*, 2002. **99**(24): p. 15313-15317.
142. Matsuoka, Y. and B. Nordén, Linear dichroism studies of nucleic acids. II. Calculation of reduced dichroism curves of A-and B-form DNA. *Biopolymers*, 1982. **21**(12): p. 2433-2452.
143. Svensson, F.R., P. Lincoln, B. Nordén, and E.K. Esbjörner, Retinoid chromophores as probes of membrane lipid order. *J. Phys. Chem. B*, 2007. **111**(36): p. 10839-10848.
144. McLachlan, J.R.A., D.J. Smith, N.P. Chmel, and A. Rodger, Calculations of flow-induced orientation distributions for analysis of linear dichroism spectroscopy. *Soft Matter*, 2013.
145. Nordén, B., Applications of linear dichroism spectroscopy. *Appl. Spectrosc. Rev.*, 1978. **14**(2): p. 157-248.
146. Stoscheck, C.M., Quantitation of protein. *Methods Enzymol.*, 1990. **182**: p. 50-68.
147. Coulter, C.B., F.M. Stone, and E.A. Kabat, The structure of the ultraviolet absorption spectra of certain proteins and amino acids. *J. Gen. Physiol.*, 1936. **19**(5): p. 739-752.
148. Goldfarb, A.R., L.J. Sidel, and E. Mosovich, The ultraviolet absorption spectra of proteins. *J. Biol. Chem.*, 1951. **193**(1): p. 397-404.
149. Goldfarb, A.R., Absorption spectrum of the peptide bond. II. Influence of chain length. *J. Biol. Chem.*, 1953. **201**(1): p. 317-320.
150. Gill, S.C. and P.H. Von Hippel, Calculation of protein extinction coefficients from amino acid sequence data. *Anal. Biochem.*, 1989. **182**(2): p. 319-326.
151. Pace, C.N., F. Vajdos, L. Fee, G. Grimsley, and T. Gray, How to measure and predict the molar absorption coefficient of a protein. *Protein Sci.*, 1995. **4**(11): p. 2411-2423.
152. Warburg, O. and W. Christian, Insulation and crystallisation of the fermenting process of Enolase. *Biochem. Z.*, 1942. **310**(6): p. 384-421.

153. Lowry, O.H., N.J. Rosebrough, A.L. Farr, and R.J. Randall, Protein measurement with the Folin phenol reagent. *J. Biol. Chem.*, 1951. **193**(1): p. 265-275.
154. Bradford, M.M., A rapid and sensitive method for quantitation of microgram quantities of protein utilizing the principle of protein-dye binding. *Anal. Biochem.*, 1976. **72**(1-2): p. 248-254.
155. Folin, O. and W. Denis, On phosphotungstic-phosphomolybdic compounds as color reagents. *J. Biol. Chem.*, 1912. **12**(2): p. 239-243.
156. Wu, H., A new colorimetric method for the determination of plasma proteins. *J. Biol. Chem.*, 1922. **51**(1): p. 33-39.
157. Legler, G., C.M. Mullerplatz, M. Mentgeshettkamp, G. Pflieger, and E. Julich, On the chemical basis of the Lowry protein determination. *Anal. Biochem.*, 1985. **150**(2): p. 278-287.
158. Smith, P.K., R.I. Krohn, G.T. Hermanson, A.K. Mallia, F.H. Gartner, M.D. Provenzano, E.K. Fujimoto, N.M. Goeke, B.J. Olson, and D.C. Klenk, Measurement of protein using bicinchoninic acid. *Anal. Biochem.*, 1985. **150**(1): p. 76-85.
159. Reisner, A.H., P. Nemes, and C. Bucholtz, The use of Coomassie Brilliant Blue G250 perchloric acid solution for staining in electrophoresis and isoelectric focusing on polyacrylamide gels. *Anal. Biochem.*, 1975. **64**(2): p. 509-516.
160. Chial, H.J., H.B. Thompson, and A.G. Splittgerber, A spectral study of the charge forms of Coomassie blue G. *Anal. Biochem.*, 1993. **209**(2): p. 258-266.
161. Compton, S.J. and C.G. Jones, Mechanism of dye response and interference in the Bradford protein assay. *Anal. Biochem.*, 1985. **151**(2): p. 369-374.
162. Chial, H.J. and A.G. Splittgerber, A comparison of the binding of Coomassie brilliant blue to proteins at low and neutral pH. *Anal. Biochem.*, 1993. **213**(2): p. 362-369.
163. Georgiou, C.D., K. Grintzalis, G. Zervoudakis, and I. Papapostolou, Mechanism of Coomassie brilliant blue G-250 binding to proteins: a hydrophobic assay for nanogram quantities of proteins. *Anal. Bioanal. Chem.*, 2008. **391**(1): p. 391-403.
164. Jones, L.J., R.P. Haugland, and V.L. Singer, Development and characterization of the NanoOrange (R) protein quantitation assay: A fluorescence-based assay of proteins in solution. *Biotechniques*, 2003. **34**(4): p. 850-861.

165. Zubkov, M.V., B.M. Fuchs, H. Eilers, P.H. Burkill, and R. Amann, Determination of total protein content of bacterial cells by SYPRO staining and flow cytometry. *Appl. Environ. Microbiol.*, 1999. **65**(7): p. 3251-3257.
166. Berggren, K., E. Chernokalskaya, T.H. Steinberg, C. Kemper, M.F. Lopez, Z. Diwu, R.P. Haugland, and W.F. Patton, Background-free, high sensitivity staining of proteins in one- and two-dimensional sodium dodecyl sulfate-polyacrylamide gels using a luminescent ruthenium complex. *Electrophoresis*, 2000. **21**(12): p. 2509-2521.
167. Berggren, K., T.H. Steinberg, W.M. Lauber, J.A. Carroll, M.F. Lopez, E. Chernokalskaya, L. Zieske, Z.J. Diwu, R.P. Haugland, and W.F. Patton, A luminescent ruthenium complex for ultrasensitive detection of proteins immobilized on membrane supports. *Anal. Biochem.*, 1999. **276**(2): p. 129-143.
168. Liu, J., Y.Z. Hsieh, D. Wiesler, and M. Novotny, Design of 3-(4-carboxybenzoyl)-2-quinolinecarboxaldehyde as a reagent for ultrasensitive determination of primary amines by capillary electrophoresis using laser fluorescence detection. *Anal. Chem.*, 1991. **63**(5): p. 408-412.
169. Bell, P.J.L. and P. Karuso, Epicocconone, a novel fluorescent compound from the fungus *Epicoccum nigrum*. *J. Am. Chem. Soc.*, 2003. **125**(31): p. 9304-9305.
170. You, W.W., R.P. Haugland, and D.K. Ryan, 3-(4-carboxybenzoyl)quinoline-2-carboxaldehyde, a reagent with broad dynamic range for the assay of proteins and lipoproteins in solution. *Anal. Biochem.*, 1997. **244**(2): p. 277-282.
171. Coghlan, D.R., J.A. Mackintosh, and P. Karuso, Mechanism of reversible fluorescent staining of protein with epicocconone. *Org. Lett.*, 2005. **7**(12): p. 2401-2404.
172. Viovy, J.L., *Electrophoresis of DNA and other polyelectrolytes: Physical mechanisms*. *Rev. Mod. Phys.*, 2000. **72**(3): p. 813-872.
173. Svensson, H., Isoelectric fractionation, analysis and characterization of ampholytes in natural pH gradients. II. Buffering capacity and conductance of isoionic ampholytes. *Acta Chem. Scand.*, 1962. **16**(2): p. 456-466.
174. Shapiro, A.L., E. Vinuela, and J.V. Maizel, Molecular weight estimation of polypeptide chains by electrophoresis in SDS-polyacrylamide gels. *Biochem. Biophys. Res. Commun.*, 1967. **28**(5): p. 815-820.
175. Stellwagen, N.C., *Electrophoresis of DNA in agarose gels, polyacrylamide gels and in free solution*. *Electrophoresis*, 2009. **30**(S1): p. S188-S195.
176. Görg, A., G. Boguth, C. Obermaier, A. Posch, and W. Weiss, Two-dimensional polyacrylamide electrophoresis with immobilized pH gradients

- in the first dimension (IPG-DALT) - The state of the art and the controversy of vertical *versus* horizontal systems. *Electrophoresis*, 1995. **16**(7): p. 1079-1086.
177. Acevedo, F., V. Marín, and M. Wasserman, Electrophoretic size separation of proteins treated with sodium dodecyl sulphate in 1-percent agarose gels. *Electrophoresis*, 1995. **16**(8): p. 1394-1400.
178. Braun, R.J., N. Kinkl, M. Beer, and M. Ueffing, Two-dimensional electrophoresis of membrane proteins. *Anal. Bioanal. Chem.*, 2007. **389**(4): p. 1033-1045.
179. Reisinger, V. and L.A. Eichacker, Solubilization of membrane protein complexes for blue native PAGE. *J. Proteomics*, 2008. **71**(3): p. 277-283.
180. Luche, S., V. Santoni, and T. Rabilloud, Evaluation of nonionic and zwitterionic detergents as membrane protein solubilizers in two-dimensional electrophoresis. *Proteomics*, 2003. **3**(3): p. 249-253.
181. Heuberger, E.H.M.L., L.M. Veenhoff, R.H. Duurkens, R.H.E. Friesen, and B. Poolman, Oligomeric state of membrane transport proteins analyzed with blue native electrophoresis and analytical ultracentrifugation. *J. Mol. Biol.*, 2002. **317**(4): p. 591-600.
182. Werhahn, W. and H.P. Braun, Biochemical dissection of the mitochondrial proteome from *Arabidopsis thaliana* by three-dimensional gel electrophoresis. *Electrophoresis*, 2002. **23**(4): p. 640-646.
183. Qiu, H. and M. Caffrey, The phase diagram of the monoolein/water system: metastability and equilibrium aspects. *Biomaterials*, 2000. **21**(3): p. 223-234.
184. Kaasgaard, T. and C.J. Drummond, Ordered 2-D and 3-D nanostructured amphiphile self-assembly materials stable in excess solvent. *Phys. Chem. Chem. Phys.*, 2006. **8**(43): p. 4957-4975.
185. Carlsson, N., K. Lundberg, C. Stenqvist, E. Westas, and B. Åkerman, *Unpublished*.
186. Rädler, J.O., I. Koltover, T. Salditt, and C.R. Safinya, Structure of DNA-cationic liposome complexes: DNA intercalation in multilamellar membranes in distinct interhelical packing regimes. *Science*, 1997. **275**(5301): p. 810-814.
187. Salditt, T., I. Koltover, J.O. Rädler, and C.R. Safinya, Two-dimensional smectic ordering of linear DNA chains in self-assembled DNA-cationic liposome mixtures. *Phys. Rev. Lett.*, 1997. **79**(13): p. 2582-2585.
188. Koltover, I., T. Salditt, J.O. Rädler, and C.R. Safinya, An inverted hexagonal phase of cationic liposome-DNA complexes related to DNA release and delivery. *Science*, 1998. **281**(5373): p. 78-81.

189. Maier, B. and J.O. Rädler, Conformation and self-diffusion of single DNA molecules confined to two dimensions. *Phys. Rev. Lett.*, 1999. **82**(9): p. 1911-1914.
190. Michanek, A., M. Björklund, T. Nylander, and E. Sparr, ssRNA base pairing at a bilayer interface can be controlled by the acyl chain order. *Soft Matter*, 2012. **8**(40): p. 10428-10438.
191. Cárdenas, M., J. Campos-Téran, T. Nylander, and B. Lindman, DNA and cationic surfactant complexes at hydrophilic surfaces. An ellipsometry and surface force study. *Langmuir*, 2004. **20**(20): p. 8597-8603.
192. Ainalem, M.-L., N. Kristen, K.J. Edler, F. Höök, E. Sparr, and T. Nylander, DNA binding to zwitterionic model membranes. *Langmuir*, 2010. **26**(7): p. 4965-4976.
193. Ekwall, P., I. Danielsson, and L. Mandell, Assoziations- und Phasengleichgewichte bei der Einwirkung von Paraffinkettenalkoholen an wässrigen Lösungen von Assoziationskolloiden. *Kolloid Z.*, 1960. **169**(1-2): p. 113-124.
194. Friman, R., I. Danielsson, and P. Stenius, Lamellar mesophase with high contents of water - X-ray-investigations of the sodium octanoate decanol water system. *J. Colloid Interface Sci.*, 1982. **86**(2): p. 501-514.
195. Fontell, K., L. Mandell, H. Lehtinen, and P. Ekwall, 3-Component system sodium caprylate - decanol - water .3. structure of mesophases at 20 degrees C. *Acta Polytech. Scand. Chem. Technol. Metall. Ser.*, 1968(74): p. 1-56.
196. Fontell, K., The structure of the lamellar liquid crystalline phase in Aerosol OT-water system. *J. Colloid Interface Sci.*, 1973. **44**(2): p. 318-329.
197. Hanczyc, P., B. Nordén, and B. Åkerman, DNA in a polyvinyl alcohol matrix and interactions with three intercalating cyanine dyes. *J. Phys. Chem. B*, 2011. **115**(42): p. 12192-12201.
198. Hanczyc, P., P. Lincoln, and B. Nordén, Interactions of binuclear Ruthenium(II) complexes with oligonucleotides in hydrogel matrix: Enantioselective threading intercalation into GC context. *J. Phys. Chem. B*, 2013. **117**(10): p. 2947-2954.
199. Simonson, T. and M. Kubista, DNA orientation in a shear flow. *Biopolymers*, 1993. **33**(8): p. 1225-1235.
200. Carlsson, N. and B. Åkerman, *Unpublished*.
201. Loew, L.M., Potentiometric dyes: Imaging electrical activity of cell membranes. *Pure Appl. Chem.*, 1996. **68**(7): p. 1405-1409.
202. Stern, H.A. and S.E. Feller, Calculation of the dielectric permittivity profile for a nonuniform system: Application to a lipid bilayer simulation. *J. Chem. Phys.*, 2003. **118**(7): p. 3401-3412.

203. Seelig, J. and A. Seelig, Lipid conformation in model membranes and biological membranes. *Q. Rev. Biophys.*, 1980. **13**(1): p. 19-61.
204. Duxbury, D.F., The photochemistry and photophysics of triphenylmethane dyes in solid and liquid media. *Chem. Rev.*, 1993. **93**(1): p. 381-433.
205. Laursen, B.W., J. Reynisson, K.V. Mikkelsen, K. Bechgaard, and N. Harrit, 2,6,10-Tris(dialkylamino)trioxatriangulenium salts: A new promising fluorophore. Ion-pair formation and aggregation in non-polar solvents. *Photochem. Photobiol. Sci.*, 2005. **4**(8): p. 568-576.
206. Hoff, B., E. Strandberg, A.S. Ulrich, D.P. Tieleman, and C. Posten, 2H-NMR study and molecular dynamics simulation of the location, alignment, and mobility of pyrene in POPC bilayers. *Biophys. J.*, 2005. **88**(3): p. 1818-1827.
207. Čurdová, J., P. Čapková, J. Plášek, J. Repáková, and I. Vattulainen, Free pyrene probes in gel and fluid membranes: Perspective through atomistic simulations. *J. Phys. Chem. B*, 2007. **111**(14): p. 3640-3650.
208. Yoshinaga, T., H. Hiratsuka, and Y. Tanizaki, Electronic absorption spectra of pyrene and hydroppyrenes. *Bull. Chem. Soc. Jpn.*, 1977. **50**(12): p. 3096-3102.
209. Thulstrup, E.W., J. Michl, and J.H. Eggers, Polarization spectra in stretched polymer sheets. II. Separation of  $\pi$ - $\pi^*$  absorption of symmetrical molecules into components. *J. Phys. Chem.*, 1970. **74**(22): p. 3868-3878.
210. Nordén, B., Formalistic framework of linear dichroism spectroscopy III. Simple formulas for dichroism analysis - orientation of solutes in stretched polymer matrices. *J. Chem. Phys.*, 1980. **72**(9): p. 5032-5038.
211. Luís, M.S.L., M.T.M.d.C. António, and M. Jorge, Sensing hydration and behavior of pyrene in POPC and POPC/cholesterol bilayers: A molecular dynamics study. *Biochim. Biophys. Acta, Biomembr.*, 2013. **1828**(3): p. 1094 - 1101.
212. Norman, D.G., R.J. Grainger, D. Uhrin, and D.M.J. Lilley, Location of cyanine-3 on double-stranded DNA: Importance for fluorescence resonance energy transfer studies. *Biochemistry*, 2000. **39**(21): p. 6317-6324.
213. Iqbal, A., L. Wang, K.C. Thompson, D.M.J. Lilley, and D.G. Norman, The structure of cyanine 5 terminally attached to double-stranded DNA: Implications for FRET studies. *Biochemistry*, 2008. **47**(30): p. 7857-7862.
214. Iqbal, A., S. Arslan, B. Okumus, T.J. Wilson, G. Giraud, D.G. Norman, T. Ha, and D.M.J. Lilley, Orientation dependence in fluorescent energy transfer between Cy3 and Cy5 terminally attached to double-stranded nucleic acids. *Proc. Natl. Acad. Sci. U. S. A.*, 2008. **105**(32): p. 11176-11181.

215. Urnavicius, L., S.A. McPhee, D.M.J. Lilley, and D.G. Norman, The structure of Sulfoindocarbocyanine 3 terminally attached to dsDNA via a long, flexible tether. *Biophys. J.*, 2012. **102**(3): p. 561-568.
216. Levitus, M. and S. Ranjit, Cyanine dyes in biophysical research: the photophysics of polymethine fluorescent dyes in biomolecular environments. *Q. Rev. Biophys.*, 2011. **44**(1): p. 123-151.
217. Callis, P.R., Electrochromism and solvatochromism in fluorescence response of organic dyes: A nanoscopic view, in *Advanced fluorescence reporters in chemistry and biology I: Fundamentals and molecular design*, A.P. Demchenko, Editor. 2010, Springer. p. 309-330.
218. Fare, T.L., E.M. Coffey, H. Dai, Y.D. He, D.A. Kessler, K.A. Kilian, J.E. Koch, E. LeProustt, M.J. Marton, M.R. Meyer, R.B. Stoughton, G.Y. Tokiwa, and Y. Wang, Effects of atmospheric ozone on microarray data quality. *Anal. Chem.*, 2003. **75**(17): p. 4672-4675.
219. Carlsson, N., R. Dainese, L. Kouk Yong, Y. Li, and B. Åkerman, *Unpublished*.
220. Bonde, M., H. Pontoppidan, and D.S. Pepper, Direct dye binding—A quantitative assay for solid-phase immobilized protein. *Anal. Biochem.*, 1992. **200**(1): p. 195-198.
221. Thörn, C., D.B.R.K.G. Udatha, H. Zhou, P. Christakopoulos, E. Topakas, and L. Olsson, Understanding the pH-dependent immobilization efficacy of feruloyl esterase-C on mesoporous silica and its structure-activity changes. *J. Mol. Catal. B: Enzym.*, 2013. **93**: p. 65-72.
222. Yamaguchi, A., M. Namekawa, T. Kamijo, T. Itoh, and N. Teramae, Acid-base equilibria inside amine-functionalized mesoporous silica. *Anal. Chem.*, 2011. **83**(8): p. 2939-2946.
223. Whitaker, J.E., R.P. Haugland, and F.G. Prendergast, Spectral and photophysical studies of benzo[c]xanthene dyes: Dual emission pH sensors. *Anal. Biochem.*, 1991. **194**(2): p. 330-344.
224. Ong, S.W., X.L. Zhao, and K.B. Eisenthal, Polarization of water molecules at a charged interface: second harmonic studies of the silica/water interface. *Chem. Phys. Lett.*, 1992. **191**(3-4): p. 327-335.